

FRACTURE MICROMECHANICS AS INFLUENCED BY ENVIRONMENT IN TEXTILE REINFORCED CERAMIC MATRIX COMPOSITES

Prepared by

D. L. Davidson
D. P. Nicolella

FINAL TECHNICAL REPORT
N000014-96-C-0076
SwRI Project No. 18-7943

Prepared for

Office of Naval Research
800 North Quincy Street
Arlington, Virginia 22217

June 1999

Reproduction in whole and in part is permitted for
any purpose of the United States Government



SOUTHWEST RESEARCH INSTITUTE

SAN ANTONIO
DETROIT

HOUSTON
WASHINGTON, DC

SECURITY CLASSIFICATION OF THIS PAGE

REPORT DOCUMENTATION PAGE				Form Approved OMB No. 0704-0188 Exp. Date: June 30, 1986	
1a. REPORT SECURITY CLASSIFICATION Unclassified			1b. RESTRICTIVE MARKINGS		
2a. SECURITY CLASSIFICATION AUTHORITY			3. DISTRIBUTION/AVAILABILITY OF REPORT		
2b. DECLASSIFICATION/DOWNGRADING SCHEDULE			Unlimited		
4. PERFORMING ORGANIZATION REPORT NUMBER(S) 18-7943-001			5. MONITORING ORGANIZATION REPORT NUMBER(S)		
6a. NAME OF PERFORMING ORGANIZATION Southwest Research Institute		6b. OFFICE SYMBOL (If applicable)	7a. NAME OF MONITORING ORGANIZATION Dr. Steven G. Fishman – Code 1131N Office of Naval Research		
6c. ADDRESS (City, State, and ZIP) 6220 Culebra Road, P.O. Drawer 28510 San Antonio, TX 78228-0510			7b. ADDRESS (City, State, and ZIP) 800 North Quincy Street Arlington, VA 22217-5000		
8a. NAME OF FUNDING/SPONSORING ORGANIZATION Office of Naval Research		8b. OFFICE SYMBOL (If applicable)	9. JPROCUREMENT INSTRUMENT IDENTIFICATION NUMBER N00014-96-C-0076		
8c. ADDRESS (City, State, and ZIP) 800 North Quincy Street Arlington, VA 22217-5000			10. SOURCE OF FUNDING NUMBERS		
PROGRAM ELEMENT NO.		PROJECT NO.	TASK NO.	WORK UNIT ACCESSION NO.	
11. TITLE (Include Security Classification) Fracture Micromechanics as Influenced by Environment in Textile Reinforced Ceramic Matrix Composites					
12. PERSONAL AUTHOR(S) David L. Davidson					
13a. TYPE OF REPORT FINAL		13b. TIME COVERED FROM 03/98 TO 06/99		14. DATE OF REPORT (Year, Month, Day) June 1999	
15. PAGE COUNT 83					
16. SUPPLEMENTARY NOTATION					
17. COSATI CODES			18. SUBJECT TERMS (Continue on reverse if necessary and identify by block number)		
FIELD	GROUP	SUB-GROUP	Key Words: ceramic matrix composites, textile or fabric reinforcement, crack growth mechanisms, fracture toughness, finite element modeling, micromechanics, stereoimaging technique		
19. ABSTRACT (Continue on reverse if necessary and identify by block number)					
<p>The goal of this research was a basic understanding of the factors that contribute to the fracture toughness of fabric reinforced ceramic matrix composites (CMCs). A technique was developed for measuring the fracture toughness of fabrics. The mechanical properties of matrix materials were measured using a Nanoindenter, and found to be low compared to the properties expected from matrix composition. Crack tip micromechanics, i.e., crack opening displacements and strains near the crack tip, were measured both for fabrics and from CMCs. It was found that fiber bundles move relative to each other during fracture, and that voids in the material accommodate that motion. The ability of fiber bundles to move is believed to be an important factor in developing a high fracture toughness in these materials. A finite element model was developed to simulate fabric fracture and the effects of an including matrix to form a composite. Exposure to air and Argon at 1100°C for 146 hrs. resulted in a decrease in fracture toughness of several composites evaluated. Micromechanics evaluation found no differences that could be attributed to the gas environment, so it was concluded that fiber strength degradation was the cause of lower fracture toughness.</p>					
20. DISTRIBUTION OF ABSTRACT			21. ABSTRACT SECURITY CLASSIFICATION		
<input checked="" type="checkbox"/> UNCLASSIFIED/UNLIMITED	<input checked="" type="checkbox"/> SAME AS RPT.	<input type="checkbox"/> DTIC USERS	UNCLASSIFIED		
22a. NAME OF RESPONSIBLE INDIVIDUAL David L. Davidson			22b. TELEPHONE (Include Area Code) (210) 522-2314		22c. OFFICE SYMBOL

FRACTURE MICROMECHANICS AS INFLUENCED BY ENVIRONMENT IN TEXTILE REINFORCED CERAMIC MATRIX COMPOSITES

Prepared by

D. L. Davidson
D. P. Nicolella

FINAL TECHNICAL REPORT
N000014-96-C-0076
SwRI Project No. 18-7943

Prepared for

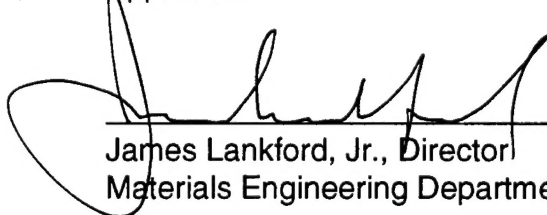
Office of Naval Research
800 North Quincy Street
Arlington, Virginia 22217

June 1999

Reproduction in whole and in part is permitted for
any purpose of the United States Government

19990701 033

Approved:



James Lankford, Jr., Director
Materials Engineering Department

FINAL TECHNICAL REPORT

March 1995 To June 1999

EXECUTIVE SUMMARY

This report summarizes work done during the entire life of this contract, but concentrates on results from March 1998 to June 1999. The objective of the research was to determine the origins of fracture toughness in fabric reinforced ceramic matrix composites. Fatigue characteristics were not studied because of work done previously.

Ceramic matrix composites (CMCs as made by several manufacturers have fracture toughness values (K_{IC}) $\geq 10 \text{ MPa}\sqrt{\text{m}}$, which is enough for some potential applications. Why are CMCs able to develop this level of fracture toughness, but why not $K_{IC} > 30 \text{ MPa}\sqrt{\text{m}}$? Why does K_{IC} degrade after exposure to high temperature air? Can these materials be "designed" for optimum fracture toughness? If so, what are the fabric and matrix characteristics that give optimum toughness?

These questions led formation of a hypothesis that fracture toughness of fabric reinforced CMCs was imparted mainly through the fabric. The matrix and interface characteristics were known to be important, although it was not understood just what values of those characteristics led to developing high fracture toughness. No quantitative understanding of how altering the characteristics of the interface and matrix altered fracture toughness. To pursue the hypothesis formed, research was needed to (1) measure the mechanical properties of the matrix, (2) measure the fracture toughness of the reinforcing fabric, and (3) develop a model to bring together fiber, interface, and matrix properties to predict fracture toughness. It was not apparent as to how to make the necessary measurements, nor what would be an appropriate model.

The mechanical properties of the matrix were measured at Oak Ridge National Laboratory using a nanoindenter in collaboration with Dr. George Pharr as part of the SHaRE Program. The matrices of several composites

in the "as received" condition and after exposure to elevated temperatures were probed. It was found (1) that modulus and hardness of the matrix materials were much lower than expected from their chemical compositions, and (2) that exposure to high temperature air lowered further those properties.

A new technique was developed for measuring the fracture toughness of fabrics because no method was found to exist for that purpose. In developing the technique, inexpensive and readily available fabrics were tested. Fracture toughness was found to be independent of crack length, which is one measure of a successful technique for toughness measurement as a material property. This result was supplemented by measurement of the micromechanical behavior of the fabric in the region of the crack tip using the stereoimaging technique. That analysis helped to confirm that a material characteristic was, in fact, being measured by the new technique. The fracture toughness of Nicalon fabric, which was used in the CMCs being evaluated, was not measured because of the expense of the fabric. Fabric architecture was shown to be very important to the tearing behavior of the fabric, although a systematic investigation of this factor was not made due to the unavailability of the desired architectures in inexpensive fabrics.

The micromechanics of the CMCs was measured during fracture by conducting experiments inside the scanning electron microscope using a loading stage. Photographs made as a function of load were analyzed using the stereoimaging technique (automated). From the displacements measured, strains were calculated. It was found that fibers and fiber bundles moved relative to one another during the fracture process, developing something akin to a "plastic zone." The high level of fracture toughness can partly be attributed to the motion of these microstructural elements which allows the high stress at the crack tip to be distributed over several fiber bundles. The fiber bundle architecture and the level of voids within the CMC affect this process considerably. No effect of exposure to high temperature in air or Argon affected the micromechanics measurements.

Finite element models were developed for (1) simulating the fabric fracture toughness experiments and (2) predicting the effects of fiber and matrix characteristics and fabric architecture on the fracture toughness of CMCs. First, the experiment to measure fabric fracture toughness was modeled. To fit with experimentally measured crack opening displacements and strains near the crack tip, the model was changed a number of times, and it became rather complex in the process, but finally, the fabric characteristics were modeled with some success. This result formed the basis of another model that simulated the CMC.

A finite element model for a CT specimen of a plain weave fabric reinforced CMC was then constructed to compare with the results of the experimental micromechanics evaluation. The model correctly predicts that some of the features identified from the micromechanics evaluation are important to the level of fracture toughness developed in the CMC, although more work on the model is needed because some of the experimental observations were not included in the model.

TABLE OF CONTENTS

Subject

Report Document Page

EXECUTIVE SUMMARY

TABLE OF CONTENTS

**THE FRACTURE TOUGHNESS OF FABRIC AS COMPOSITE REINFORCEMENTS
(Manuscript 1)**

**FRACTURE TOUGHNESS MICROMECHANICS OF CERAMIC MATRIX
COMPOSITES FABRIC REINFORCED (Manuscript 2)**

**FINITE ELEMENT MODELING OF FRACTURE TOUGHNESS IN FABRIC
REINFORCED CERAMIC MATRIX COMPOSITES (Manuscript 3)**

CONCLUSIONS

PUBLICATIONS

THE FRACTURE TOUGHNESS OF FABRICS AS COMPOSITE REINFORCEMENTS

D.L. Davidson, D.P. Nicolella, and B.S. Spigel
Southwest Research Institute
San Antonio, TX 78228

ABSTRACT

An experimental technique has been developed to measure the fracture toughness of fabrics using the variables normally associated with fracture mechanics: stress and crack length. The technique uses an expandable cylinder around which the fabric with a slit (crack) of known length is wrapped. Pneumatic pressure is used to apply stress to the fabric until the crack propagates. Fracture toughness was found to be independent of initial crack length within limits. It has been possible to evaluate only one specimen geometry, so it is not known with certainty that a material characteristic is being measured. Crack tip micromechanics measurements were made during the toughness experiments, and these results were compared with a finite element model of the experiment. Crack opening displacement and the distribution of effective strain ahead of the crack tip were in reasonable agreement when fiber sliding was included in the FEM. The conclusion is that a crack in fabric may be characterized by linear elastic fracture mechanics, and that fracture toughness can be used as a description of fabric damage tolerance.

INTRODUCTION

Fabrics have been used increasingly as structural materials, first as coated materials in belts, sails, pressure suits, balloons, etc., but more recently in composites, both polymer and ceramic matrix materials. In the period before fracture mechanics was developed, several studies of crack growth in fabrics were published [1-4]. The last of these studies by Ko [4] was performed at Southwest Research in 1975. Various methods were used by these investigators to measure useful engineering properties, but the concepts of fracture mechanics were not applied. Batra, et al. [5] did use fracture

mechanics concepts to explore the tearing of spunbound fiberweb fabrics and found that the measured fracture toughness was independent of crack length for double edge notched specimens, within certain limits of crack lengths. The fracture toughness of a similar material, paper, has been investigated by a number of investigators [6]. Continued application of woven fabrics in composite materials has caused determination of a fracture mechanics approach to be reconsidered, because the design of a composite material from a fracture perspective starts with a knowledge of the fracture properties of the constituents.

The development of a high level of fracture toughness in metallic alloys depends on the formation of a plastic zone near the crack tip. When a cracked body is loaded, stress concentrates at the crack tip, which causes the metal to deform, thereby lowering the stress concentration because load is distributed over a larger area. Thus, the crack is "shielded" from the stress concentration. Provided the plastic zone is small relative to crack length, the fracture of the material may be described by linear elastic fracture mechanics (LEFM). How does a fabric reinforced material develop fracture toughness, and can fracture of a fabric be described by LEFM? This paper presents a procedure for measuring experimentally the fracture toughness of fabric reinforced materials, together with a model of material behavior that can assist in determining how fracture toughness is developed, and perhaps ways of increasing it.

ANALYSIS

The geometry of a fabric has the effect of dividing the continuum of the metallic alloy into discrete load bearing elements, each represented by fiber bundles (tows). Consider the standard fracture toughness specimens, such as a center cracked panel (CCP) or double edge notched (DEN) specimen made from plane weave (PW) fabric. When a load is applied perpendicular to the crack in the direction of one of the orthogonal sets of fibers, it is divided evenly between the uncut fibers. If loaded to failure, the tensile strengths of individual fibers, or tows, are tested; cut fiber tows support no load, and stress is not concentrated at the crack tips, unless the fixture through which load is applied is compliant. A "crack opening displacement" (COD) develops because the uncut fibers stretch elastically, while those cut do not. Thus, a "fracture toughness test"

of this type of specimen actually tests the strength of a number of fibers that are loaded in parallel. Fibers perpendicular to the loading direction experience, to a first approximation, no increased stress. There is no rotation of fibers in one direction relative to fibers in the other. As Ko discovered [4], the compliance of the end plates through which the fabric is loaded affects the level of crack opening in the specimen.

Now consider the geometry of a compact tension (CT) specimen, where the load line is offset from the crack tip. When loaded, the bending that accompanies the CT specimen design will cause rotation between the orthogonally oriented fibers until they interfere with each other. Further displacement of the loading points results in out-of-plane buckling that will continue to increase until the loading points have rotated so that they line up with the first line of unbroken fibers. Further loading will stress this first fiber row until it breaks, allowing further rotation of the load line into a position above and below the second row of fibers that subsequently break, etc., and tearing of the fabric continues.

If the open space of the fabric is filled with a material of low modulus or low strength, then fibers along the crack flank are not as free to rotate; thus, each half of the specimen is stiffer and acts more as a beam, and that transfers more of the load ahead of the crack tip so that it is distributed more evenly amongst at least several rows of fibers. Thus, fiber loading is not concentrated only on the first row of fibers, and the distribution of fiber stresses approaches more closely that of a metallic material.

If this analysis is correct, then the role of the composite matrix, in the narrow context of fracture toughness, is to fill the interstices of the fabric, which prevents the rotation of fibers relative to one another. The consequences of this function for the matrix are:

Either: (1) the compressive, or crushing, strength of the matrix is an important property.

(2) The modulus of the matrix is important, especially if it only deforms elastically when subjected to shearing stresses.

(3) Rotations of fibers relative to each other and sliding of fibers against each other are expected to increase fracture toughness because of load sharing amongst fibers that results from these motions.

(4) The level of porosity in the composite is a critical factor in controlling fracture toughness because it permits fiber and fiber bundle relative motion.

(5) If the matrix adheres to the fibers and fiber bundles, the relative motion of fibers and bundles near a crack tip would be prevented., concentratiang the load. Conversely, if the matrix adheres to the fiber bundles, it can help carry the load, thereby lowering the stress on the fibers.

(6) The effect of oxidation on the matrix properties may strongly influence fracture toughness if oxidation increases the volume of the matrix, which would limit relative fiber rotations.

HYPOTHESIS

The foregoing analysis leads to the hypothesis that fracture toughness of fabric reinforced composites is dependent principally on the fracture toughness of the fabric, and is limited by the presence of the matrix. The matrix usually decreases toughness because it prevents fibers and fiber bundles from rotating and sliding relative to one another, thus limiting the load sharing capacity of fibers and fiber bundles in the zone of high stress at the crack tip. Using a fabric with high fracture toughness is important in developing fracture toughness of fabric reinforced composites, but the effectiveness of the fabric will be limited if the matrix characteristics are not optimal. If the fracture toughness of a composite is to be predicted, then it will be necessary to know (1) the fracture toughness of the reinforcing fabric, and (2) the characteristics of the matrix that will minimize toughness loss.

CONCEPT

The experimental apparatus shown in **Fig. 1** was inspired by a failure analysis of a "G" suit worn by pilots during aerobatic maneuvers. In essence, this suit is a pressure vessel made from

fabric. Applied pressure tensions the suit and prevents blood accumulation in the legs of the pilot during maneuvers. In the failure, the material in the leg of the suit had split by Mode I tearing during pressurization. The apparatus shown in the figure simulates this loading of the fabric, and allows the Mode I fracture toughness of a fabric to be measured. This concept is a refinement of that used by Topping [3].

The device shown in the figure consists of an inflatable cylinder that is wrapped with the fabric of interest that is held in place by clamps. A slit (crack) is introduced into the fabric by cutting. The cylinder is a bladder (presently the intertube from a motorcycle tire), whose diameter can be increased by internal pressure. The diameter is fixed on each end by a clamp. The area beneath the slit is reinforced with a metallic or polymeric membrane to prevent excessive out-of-plane bulging during pressurization. Out-of-plane motion near the crack is further suppressed by the transparent plate that is held tangential to the cylinder.

When the cylinder is pressurized, fibers are tensioned in the hoop stress direction. Fibers that have been cut by the slit do not develop the level of hoop stress of the uncut fibers, and the result is that the slit opens (crack opening displacement), which causes stress to be concentrated on the fibers at the ends of the slit (crack tip stress concentration). Also part of the experimental apparatus is a video camera that images the crack tip region at an appropriate magnification. For the experiments described here, 4 times was found to be a useful magnification. The video images were captured using a Macintosh computer, providing a complete record of changes in the crack tip region.

As pressure is increased, crack opening displacement (COD) increases until the fiber or fiber bundle at the crack tip breaks when its tensile strength is exceeded. The slit then elongates by successive failure of fibers. When the experiment is carefully conducted, the output of a pressure transducer records the load at which the fabric just begins to tear from the crack tip, and fracture toughness is computed from the energy release rate concepts of fracture mechanics using the following equation

$$K_c^2 = EG_c = \pi\sigma_c^2 a \quad (1)$$

where K_c = fracture toughness, E = elastic (Young's) modulus, G_c = energy release rate, σ_c = remotely applied stress level when the crack begins to grow, and a = half the crack length.

For the configuration shown in Fig. 1, σ = hoop stress, as computed from

$$\sigma = pR/t \quad (2)$$

where p = pressure in the cylinder, R = cylinder radius, and t = thickness of the fabric.

Therefore fracture toughness is

$$K_c = (pR/t)\sqrt{\pi a} \quad (3)$$

The assumption is made that any friction between the cylinder and fabric has a negligible effect on the results.

FRACTURE TOUGHNESS EXPERIMENTS

Fabric: The fabric chosen for evaluating this fracture toughness test concept was an inexpensive cotton - polyester blend of plane weave architecture. The "microstructure" of the fabric is shown in Fig. 2 in a no load condition. The diameter of each fiber bundle was measured as approximately 0.5 mm in a slightly taught condition. Fibers are centered approximately each 0.5 mm. The fraction of fiber tows in the fabric is approximately 90%, as seen in Fig. 2. The load elongation curve for a typical fiber tow is shown in Fig. 3, from which two elastic moduli were computed, $E_1 = 200$ MPa and $E_2 = 400$ MPa. The initial, low modulus E_1 is due to the straightening of kinks in the fiber that resulted from its having been woven. Fracture stress of a typical fiber was determined to be approximately 20 MPa. Statistically meaningful values of these parameters have not been measured. Also, some creep of the fibers at high loads was noticed during testing.

Fracture Toughness Results: The concepts of eqs. (1) - (3) were tested by performing experiments with cracks (slits) of different

lengths. The critical stress to propagate the crack was determined from the pressure required to propagate the crack.

The correlation between computed K_c and crack length ($2a$) is shown in **Fig. 4**. The measurements indicate that K_c is probably independent of crack length. The variations in toughness were caused by variations in the strength of fiber bundles and inaccuracies in measurements of load and crack length. This result provides confirmation that the use of the energy release rate concept is valid for this configuration, although further experiments using a fabric having a low variation in the distribution of fiber strengths would be helpful.

Typically, fracture toughness has been considered to be a material parameter when two different specimen configurations yield the same value. Use of this concept has not been possible with fabric because of limitations in specimen configuration, as considered in the introduction. To compensate for this limitation, efforts were made to examine the micromechanics of the crack tip.

MEASUREMENT OF DISPLACEMENTS AROUND THE CRACK TIP

Several images from the fabric being loaded to the point of tearing, then in the tearing mode, are shown in **Fig. 5**. Shown in the figure are a few of the many images digitally stored during the course of a fracture toughness experiment. The displacements caused by loading can be measured by comparison of these images against the image at minimum load. Measurements were assisted by addition of the random pattern of dots seen in the crack tip region.

Crack opening displacement (COD) and strains ahead of the crack tip provide additional information about the micromechanics of crack initiation and growth in continuum materials. For the fabric, these parameters have been measured so that they could be compared with similar information measured from other materials and with a finite element model of the fabric.

An automated imaging processing system named DISMAP [7] was used to measure in-plane displacements by comparing photographs of the crack tip region before and after loading. A typical analysis is shown in **Fig. 6**. Displacements are shown overlaying a

photograph of the crack tip region. From these displacements, the COD and three elements of the symmetric strain tensor are computed, and from these axial and shear strains, the maximum and minimum principal strains, maximum shear strain, and effective strain were computed, assuming that the fabric could be treated as a continuum solid. Some of the COD and strains measured will be compared to results of the finite element analysis.

FINITE ELEMENT ANALYSIS OF FABRIC FRACTURE

The purpose for developing a finite element model [8] was to simulate the deformation and fracture behavior of fabric reinforced composites. The model described will be used to investigate the differing contributions of the fabric and matrix to the development of fracture toughness in composite materials and to assist in the design of these composites by identifying the characteristics of the matrix that produce maximum fracture toughness.

An incremental approach was taken in developing the computational model. The initial finite element model (FEM) was for the fabric only. However, the model was formulated so that additional constituents (such as the matrix) could be added. As the model for the fabric was developed, its predictions were compared to experimental results to ensure that the essential experimental observations were being captured. The model takes advantage of the discrete nature of the fabric by depicting the fiber bundles as pin-linked beams and their intersections as joints. Comparison with experimental results indicated that it was necessary to allow one set of beams (a fiber bundle) to slide relative to the crossing beam (fiber bundle).

Methods: A one-quarter symmetry model was used to take advantage of the symmetry in the experimental configuration, and reduce computational cost. The quarter scale model consisted of an area of fabric with a slit on the vertical centerline splitting the model horizontally in the center. The mesh consists of slender beams representing the fiber tows connected by rotational pin joints at each fiber intersection. The fibers tows were 0.5 mm in diameter and were spaced 0.5 mm apart, which simulates the fabric architecture shown in Fig. 2. Each individual tow in the fabric was

modeled as a slender beam with a circular cross section. Each beam was connected to its neighboring beams using pins joints that allowed in-plane rotation; the bending stiffness of the beam is much greater than the rotational stiffness provided at each joint. The stiffness of the fiber tows was determined from load-elongation experiments performed on individual tows; see Fig. 3. Only one modulus, the highest, was used to describe the fiber behavior. Each beam representing a fiber tow was connected at a pinned joint. These elements provided displacement constraints between elements but allowed slippage, with friction, relative to each other.

Rotational stiffness was provided at each pin joint through non-linear rotational springs. The behavior of the springs is defined by the kinematic behavior of the joints. At each joint, a non-linear torsional spring element was included to model the rotational behavior between the two orthogonal fiber tows. The torque-displacement behavior is shown in Fig. 7. An initial torsional stiffness allows for minimal rotational resistance between fibers, but when the rotation reaches the lock-up angle, the stiffness increases accordingly.

Loads corresponding to the hoop stress generated in the fabric due to the internal pressure were applied to the nodes on the edge opposite to the slit. The nodal loads were determined from:

$$F_{\text{node}} = \sigma_H A / N \quad (4)$$

where F_{node} are the applied nodal forces, σ_H is the hoop stress, A is the cross sectional area, and N is the total number of nodes. The model was solved using the commercial finite element analysis software package ABAQUS [8].

Model Results: A comparison of crack opening displacements (COD) as measured, and as determined from the model are shown in Fig. 8 as a function of distance behind the crack tip. There is reasonable agreement between model and measured values, although a more quantitative assessment in terms of pressure (stress) must be made. One difference is apparent: COD at the crack tip experimentally is not zero because of fiber tow sliding, as shown in Fig. 5, which gives the COD a "blunt crack" appearance. As the fiber tows slide away

from the crack front in the direction of loading, the tip is effectively blunted distributing the load among several fibers at the tip and just ahead. Sliding redistributes the load among fiber tows just ahead of the crack tip, thereby effectively reducing the stress on the most highly stressed fiber at the crack tip and increasing the fracture toughness of the material.

The COD data are shown in **Fig. 9** as a function of the square root of distance behind the crack tip (\sqrt{d}). For a K controlled linear elastic crack, COD vs. \sqrt{d} is linear, and the data in **Fig. 9** indicate that experiment and the FE model are linear in \sqrt{d} , excluding the "blunting" that occurs at the crack tip due to fiber sliding. This result is another indication that linear elastic fracture mechanics is applicable to the fracture of fabrics.

An experimentally determined distribution of effective strain about a crack tip is shown in **Fig. 10** (heavy, dark lines) with the strains determined from the finite element model (narrow, light lines). Only the area from the FEM that coincides with the experimental analysis is shown. The agreement is considered as good, especially near the crack tip. Quantitatively, the far field strains are about the same for experiment and model, but the strain contours are different.

The effective strains determined by experiment and FEM directly ahead of the crack tip are compared in **Fig. 11**. Strains were normalized (divided by the crack tip strain), and 0.1 mm was added to the distance axis to allow the crack tip strain to be included in the graph. The result is that the FE model is linear on a log-log plot at some distance from the crack tip. Since these data are linearly correlated, the strain field may be described by a Hutchinson, Rice & Rosengren (HRR) type function [9,10]. Closer to the crack tip, strain is somewhat non-linear, which occurs because the fibers are allowed to slide one against the other. This feature is found in the experimentally determined strains, but is not seen in the model unless fiber sliding is included. Away from the crack tip, the experimentally determined strain distribution is also linear in this plot. This is another indication that fracture mechanics may be used to describe a crack in fabric.

Qualitatively, the shape of the strain fields are in reasonable agreement, indicating that the FE model successfully captures the

essence of the loading applied to the fabric, when fiber sliding is included. The strain fields may be made to agree quantitatively by using a suitable value of failure stress in the model.

DISCUSSION

Fracture toughness as a material property is usually verified by demonstrating that K_c is independent of specimen geometry, but that requires measurements from different specimen geometries. Only one specimen configuration has been developed for measuring fracture toughness here. However, the results, Fig. 4, indicate that K_c is probably independent of the crack length (within a range of values that are dependent on the experimental apparatus used here). If K_c is independent of crack length, that implies the use of an energy release rate concept to compute K_c is relevant.

However, the data of Ko [4] were reanalyzed and K_c was computed. Those data, from CCP specimens, show that fracture toughness is also independent of crack length, except for the smallest crack lengths. If the data of Ko are valid and can be compared to the present results, then two types of fabric specimen have been tested, which helps to verify that continuum based fracture mechanics is a valid concept for describing the fracture properties of the discrete element fabric.

Since varying specimen geometry was not feasible, experimental measurements of crack opening displacement and strains ahead of the crack tip were compared to (1) continuum models of crack tip behavior, and (2) a finite element model constructed to simulate the fabric behavior.

Comparison of measured COD with those computed by the finite element model indicates that COD is linear as a function of \sqrt{d} (d = distance from the crack tip), excluding a few fiber bundle distances near the crack tip. This behavior indicates experimentally that the crack tip is K controlled and that the model is capturing this aspect of fabric behavior.

Fiber sliding is a property of the fabric that appears to be important to the development of fracture toughness, as hypothesized. Fiber

sliding must be included in the FEM to produce a good fit with experimental measurements of fiber strains.

Further testing is needed to determine the efficacy of this technique for measuring fracture toughness. A stronger bladder material may be needed to test tougher, aerospace-quality materials. A stronger bladder may also prevent or minimize out-of-plane bulging near the crack. The effects of friction between the bladder, test fabric and the restraining plate may also need to be considered in a more advanced experimental apparatus. Frictional effects could slow or deter crack growth.

CONCLUSIONS

1. A new experimental technique has been developed to measure the fracture toughness of fabric. The technique uses a fabric with a slit (crack) of known length wrapped around an expandable cylinder. Pneumatic pressure is used to apply stress to the fabric until the crack propagates.
2. The energy release concepts of fracture mechanics can be used to describe the fracture of plain weave fabric.
3. Crack opening displacement conforms to linear elastic fracture mechanics, except very near the crack tip, where fiber sliding causes the crack tip to be blunt.
4. Strains ahead of the crack tip conform to linear elastic fracture mechanics analysis, except near the crack tip. Strains in the model agree with measured strains when fiber sliding is included.
5. Based on limited experimental data for plain weave fabric, fracture toughness is probably independent of crack length. Additional testing with better quality fabrics and different weaves is needed to further substantiate this result.

ACKNOWLEDGEMENT

This work was funded by The Office of Naval Research, Dr. Steven Fishman project monitor. A discussion with Dan Benac about the G suit failure resulted in formulation of the fracture toughness experiment. John Campbell, Byron Chapa, and Jim Spencer provided able experimental assistance. The authors acknowledge discussions with, and appreciate the suggestions of, Dr. Carl Popelar.

REFERENCES

1. N. Abbot and J. Skelton, "Crack propagation in woven fabrics," J. Coated Fibrous Mats., 1972, v. 1, p. 234.
2. W. Freeston and W. Claus, "Crack propagation in woven fabrics," J. Appl. Phys., 1973, v. 44, p. 3130.
3. A. Topping, "The critical slit length of pressurized coated fabric cylinders," J. Coated Fabrics, 1973, v. 3, p. 96.
4. W.L. Ko, "Fracture behavior of a nonlinear woven fabric material," J. Comp. Materials, 1975, v. 9, pp. 361-369.
5. S. Batra, W. Pan, D. Buchanan, "Application of fracture mechanics to the tear resistance of fiberweb structures," **Proceedings of The International Symposium on Fiber Science and Technology**, Hakone, Japan, 1985. Elsevier Applied Science Publ., Barking, UK, 1985, pp. 72-73.
6. Y. Yu and P. Karenlampi, "On crack stability in paper toughness testing," J. Mat. Sci., 1997, v. 32, pp. 6513-6517.
7. E.A. Franke, D.E. Wenzel and D.L. Davidson, Rev. Sci. Instruments, 1991, v. 62, pp. 1270-1279.
8. ABAQUS v.5.6, HKS Inc., Pawtucket, RI.
9. J.W. Hutchinson, J. Mech. and Physics Solids, 1968, v. 16, pp. 13-31.
10. J. R. Rice and G.F. Rosengren, J. Mech. and Physics Solids, 1968, v. 16, pp. 1-12.

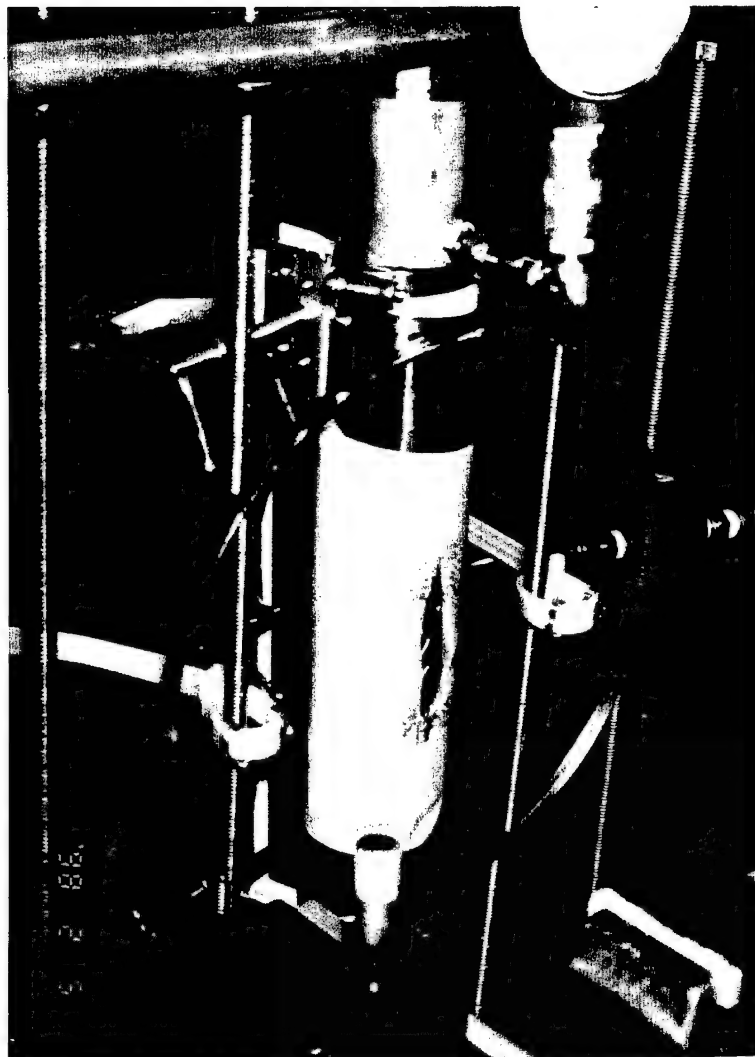


Fig. 1 Apparatus for measuring the fracture toughness of fabric. See text for a description of the concept and a description of the parts.

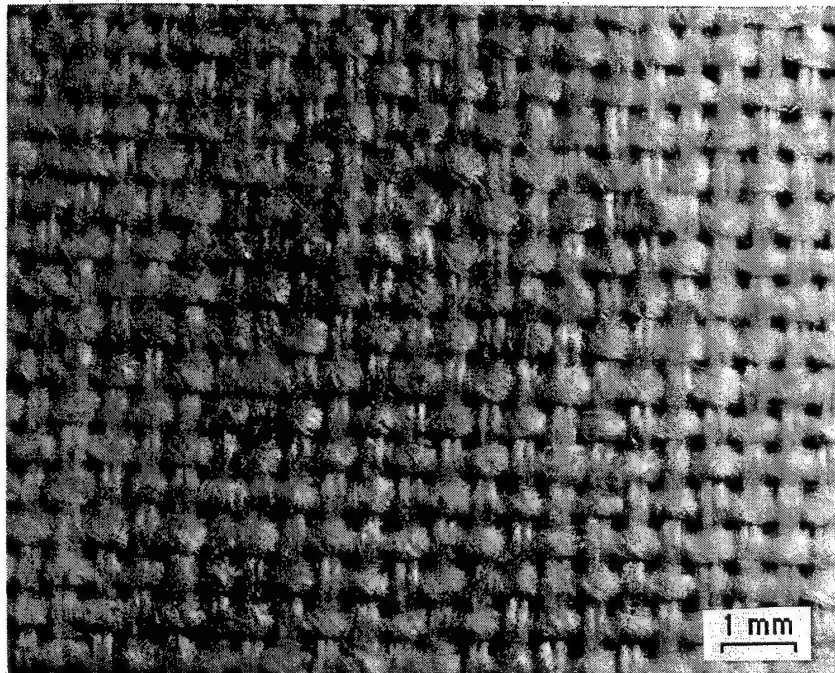


Fig. 2. Fabric "microstructure" used for evaluation of the fracture toughness measurement concepts. Plane weave, cotton fabric.

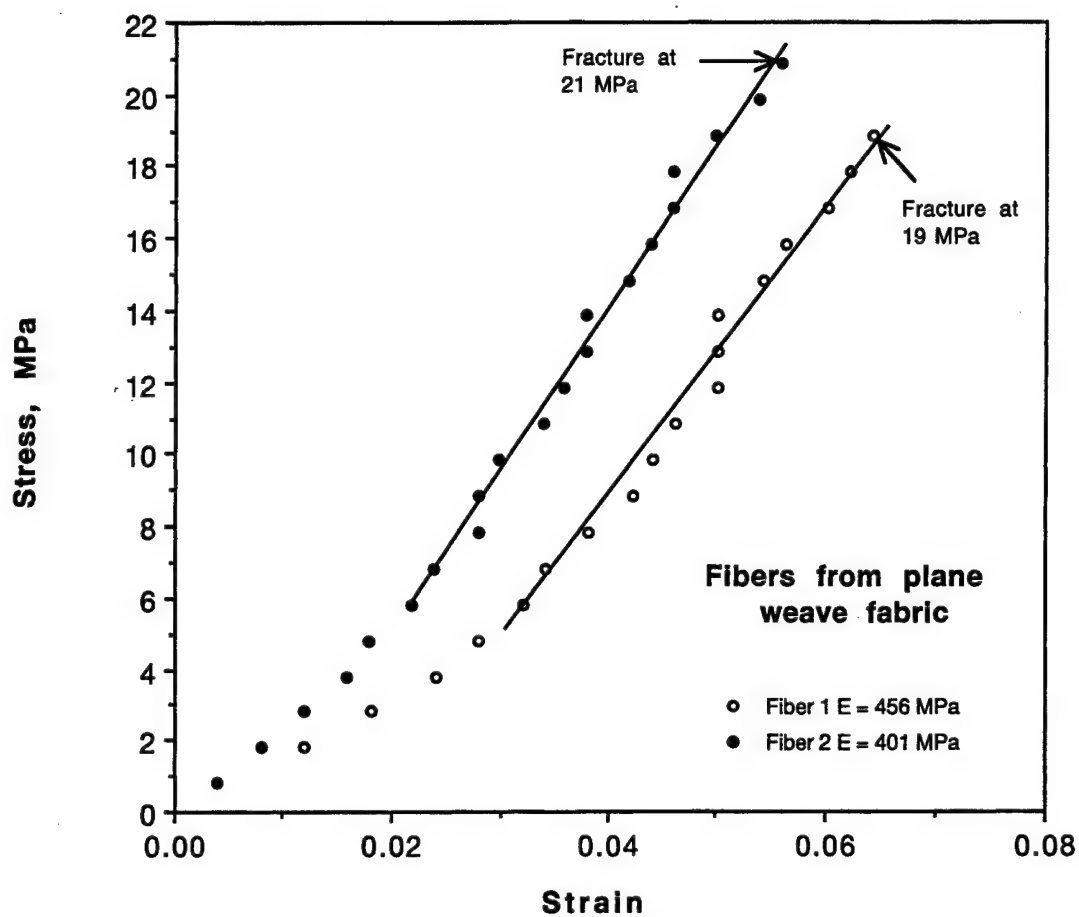


Fig. 3. Load-elongation relationship for individual fiber tows.

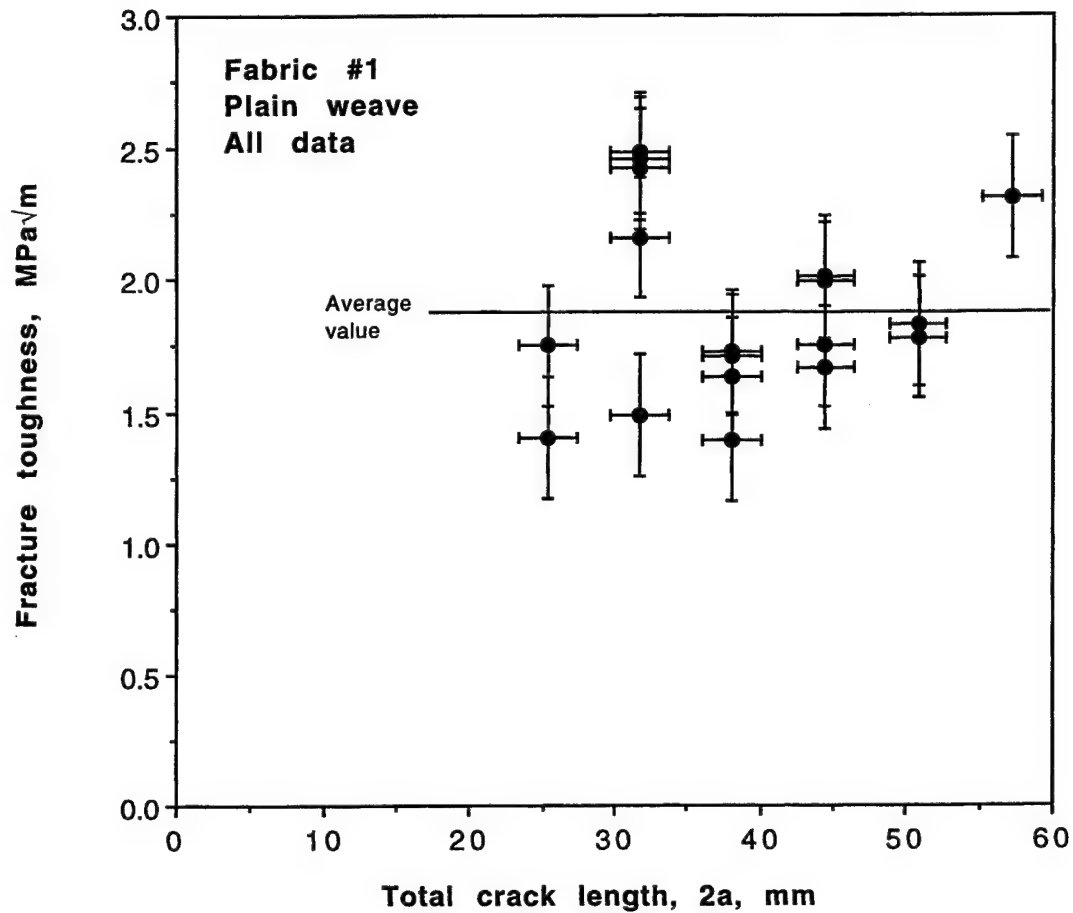


Fig. 4 Correlation of fracture toughness computed from eq. (3) with crack length. Error bars were estimated from uncertainties in pressure and crack length measurements.

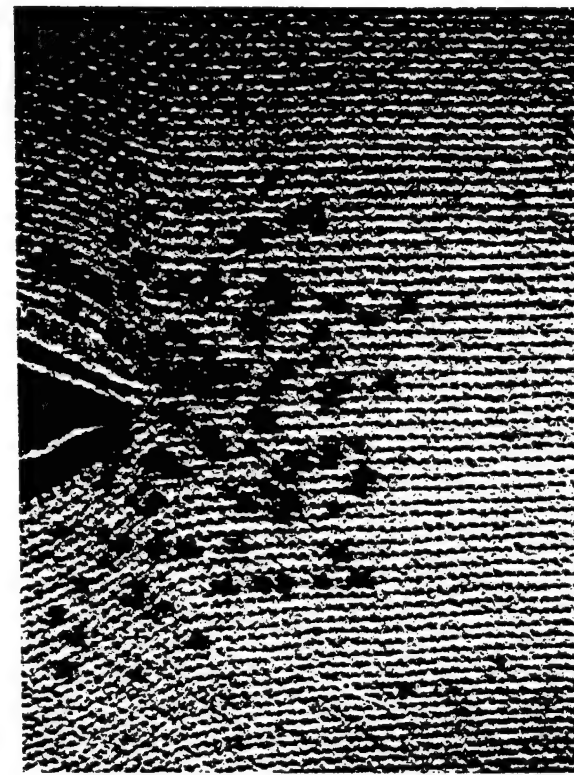
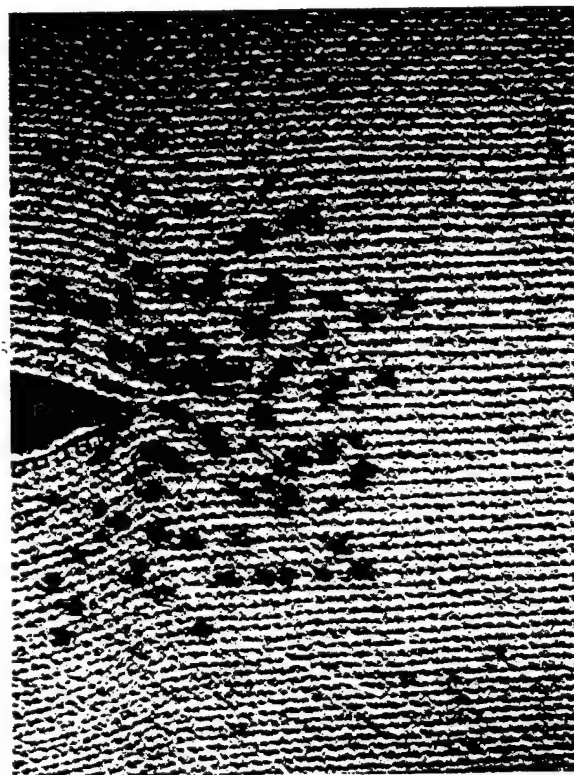
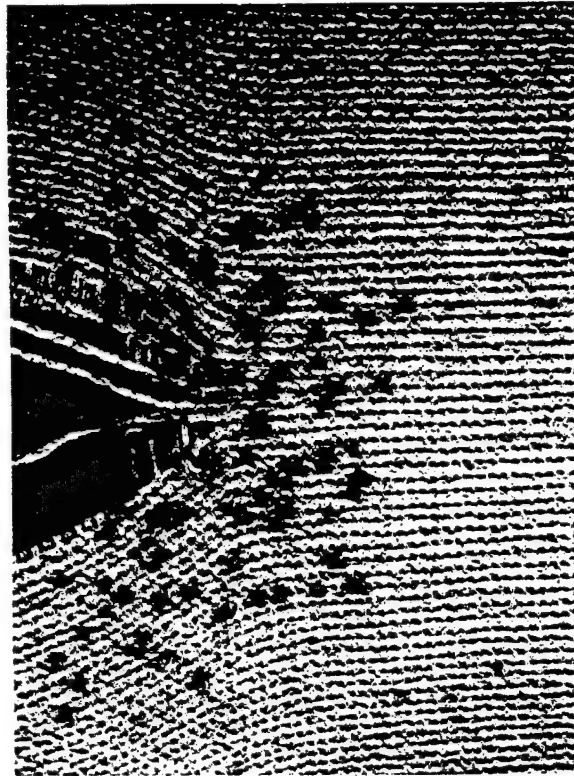
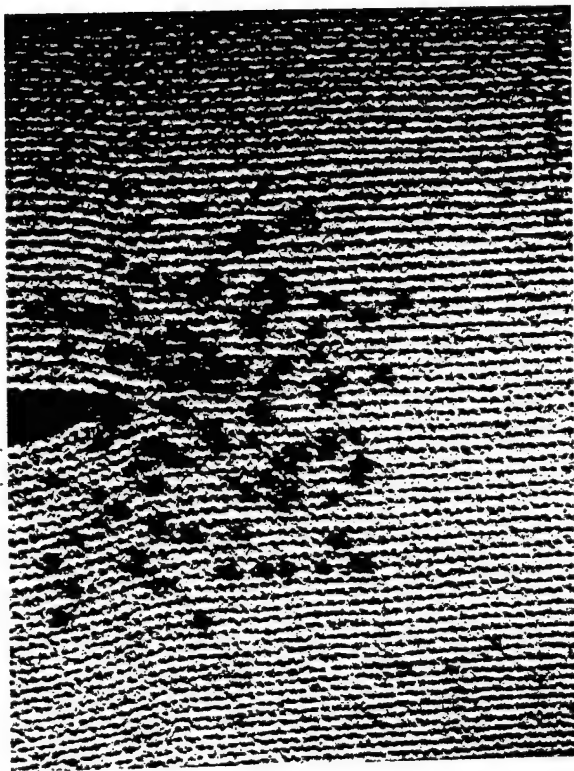


Fig. 5. Sequence of images of the crack tip with increasing pressure, showing first an increase in COD, then elongation of the crack (tearing).

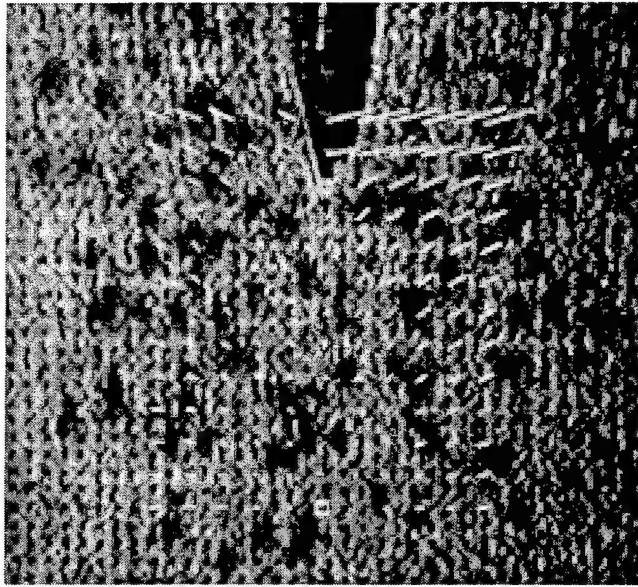


Fig. 6 Displacements overlaying a photograph of a loaded crack tip. Displacements were measured each 1 mm, and the displacements are shown 2X actual values.

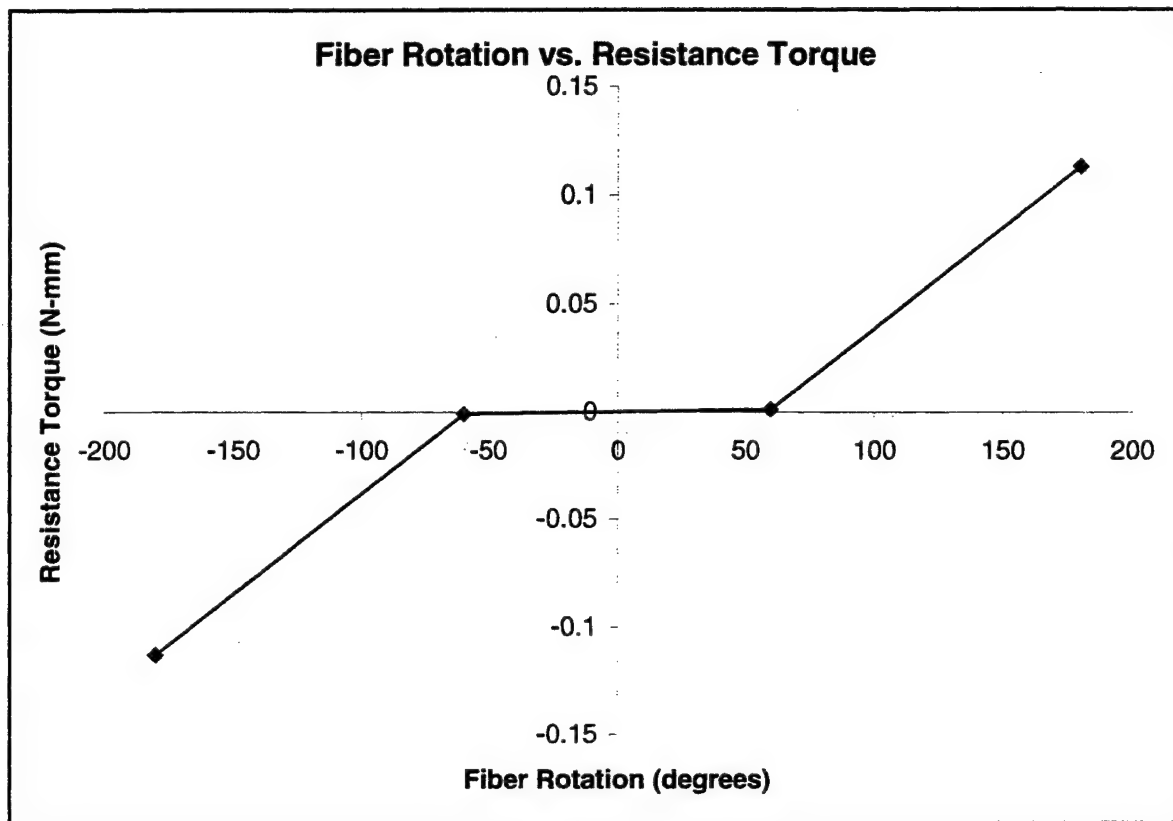


Fig. 7. Fiber rotation vs. resistance torque. The fiber tows were allowed to rotate with respect to each other up to the lock-up angle (60°) where the rotational resistance increased.

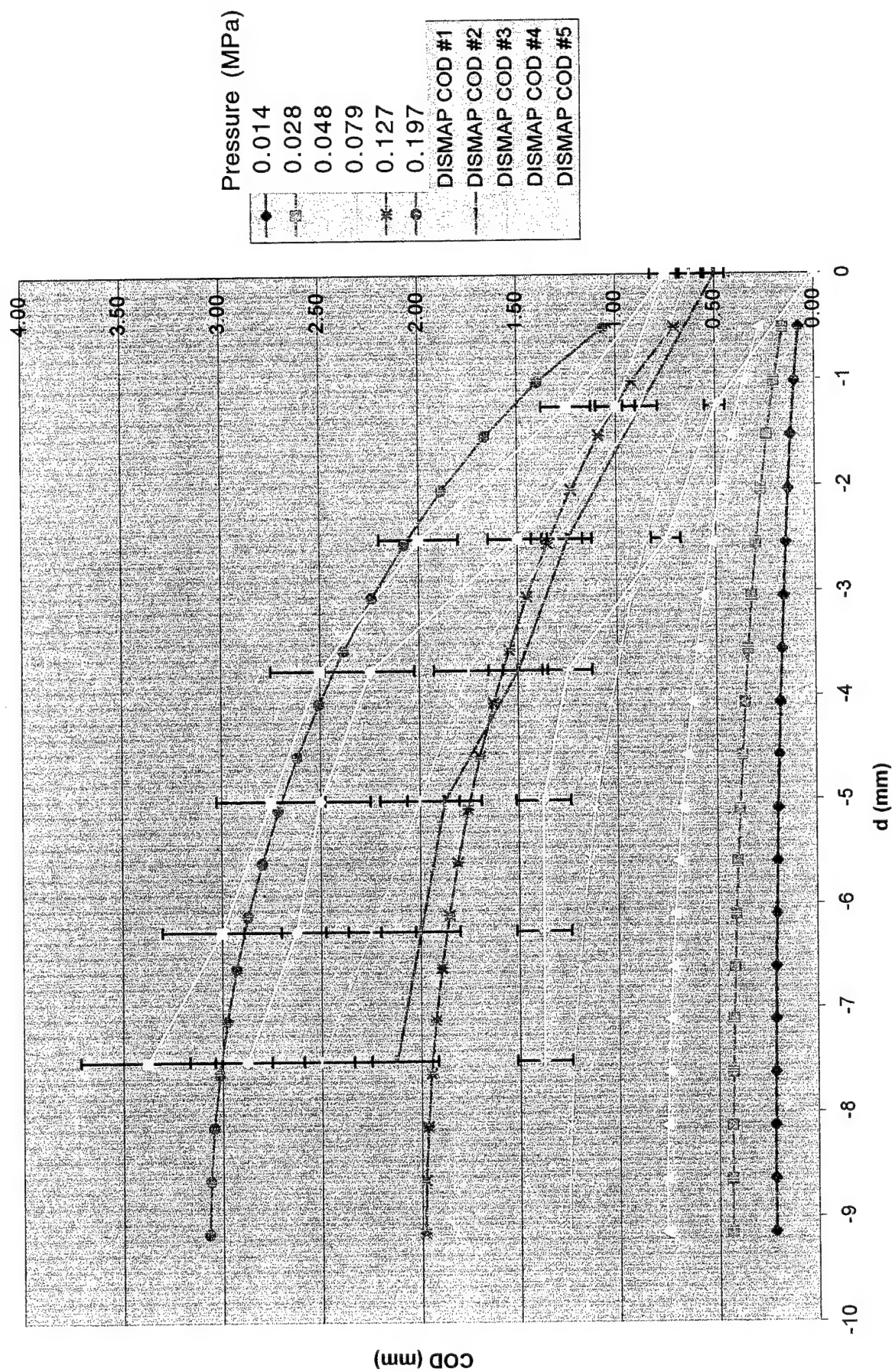


Fig. 8. Comparison of crack opening displacements (COD) as measured and computed using the finite element model as a function of distance (d) behind the crack tip.

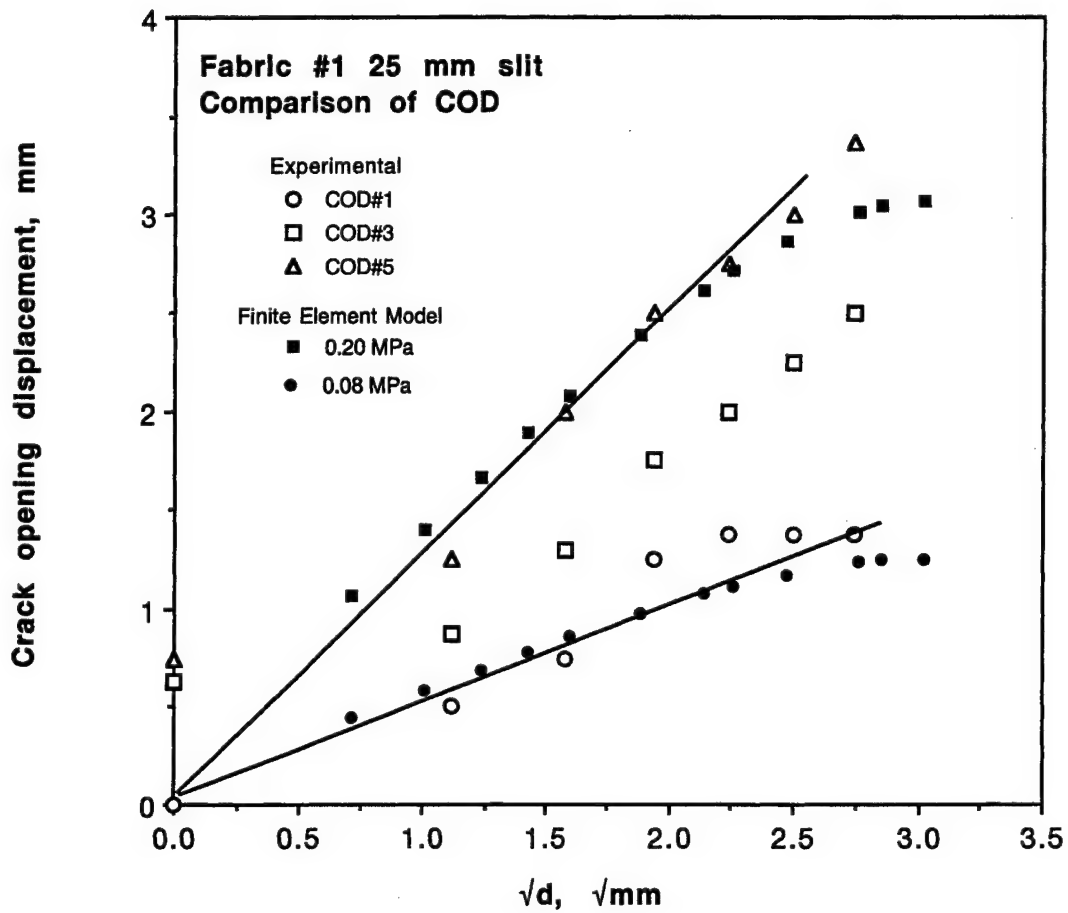


Fig. 9. Comparison of COD vs. \sqrt{d} , showing that both are linear, indicating that the crack can be described by LEFM.

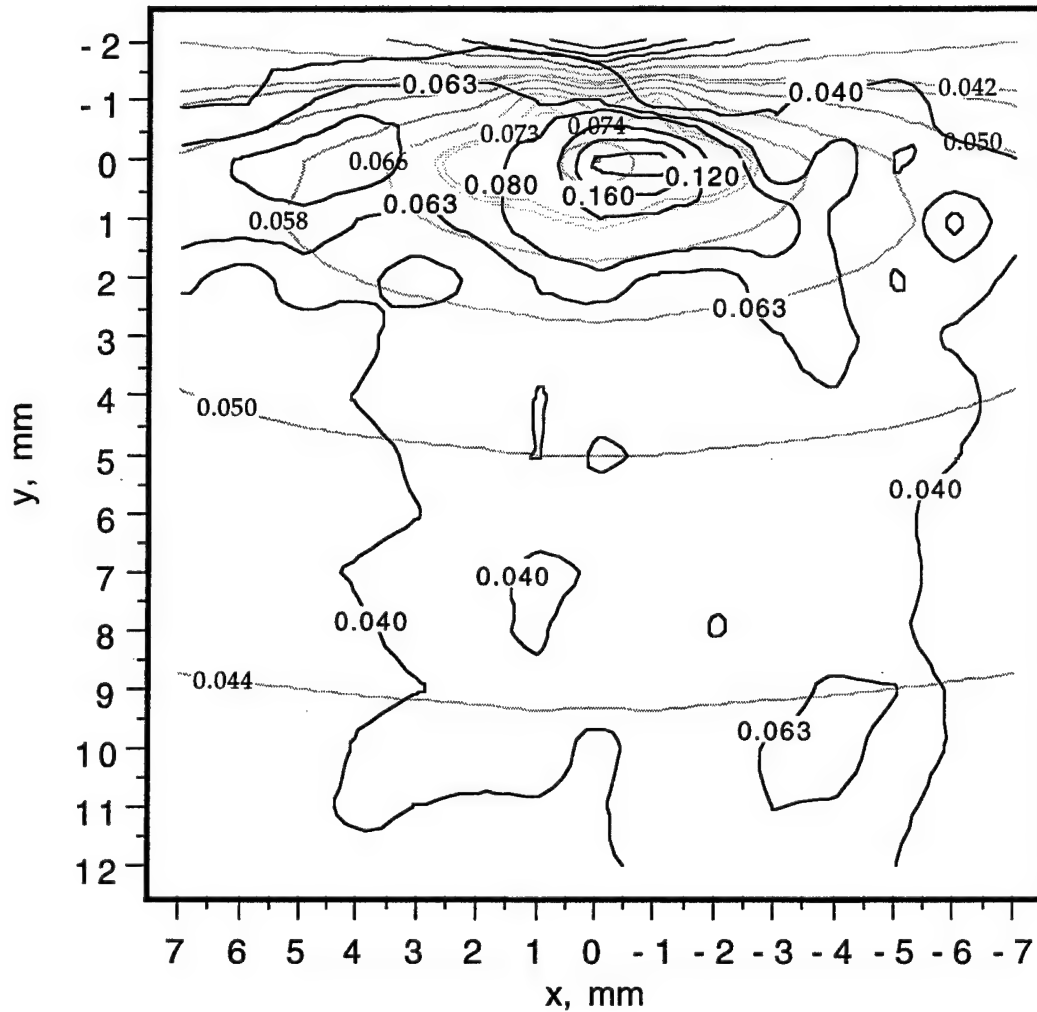


Fig. 10 Comparison of the distribution of effective strains ahead of the crack tip, as determined by experiment (heavy, dark lines and numbers), and as computed by the finite element model (light lines and small numbers). Crack enters from the top and the tip is at $x, y = 0$.

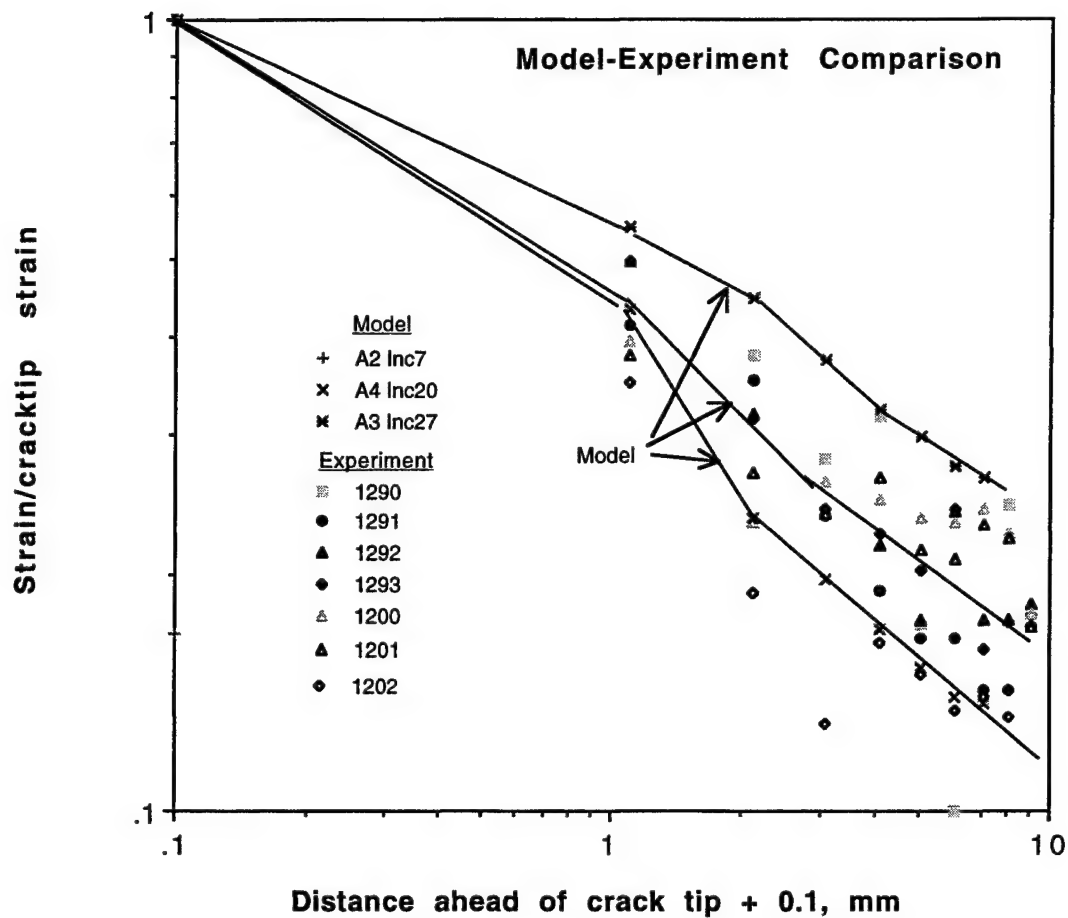


Fig. 11 Distribution of effective strains directly ahead of the crack tip. Log-log plot of normalized strain vs. distance ahead of the crack tip, showing that the correlation is approximately linear, as would be expected from fracture mechanics analysis. Addition of 0.1 mm to the distance ahead of the crack tip allows crack tip strain to be included in the graph.

FRACTURE TOUGHNESS MICROMECHANICS OF FABRIC REINFORCED CERAMIC MATRIX COMPOSITES

David L. Davidson
Southwest Research Institute
San Antonio, Texas 78228

ABSTRACT

The micromechanics of fracture of two ceramic matrix composites was investigated. The materials evaluated contained Nicalon fibers woven into fabrics (Plain Weave and 8 Harness Satin) with matrices of alumina or silicon carbide. Detailed studies at ambient temperature were performed on three conditions of each material: (1) As-received, after exposure at 1100°C for 146 hrs in (2) air, and (3) Argon. Compact tension specimens of the two materials were broken using a loading machine inside the scanning electron microscope, and displacements were measured from photographs made as loads were increased to fracture. Some effect of environment was found on the magnitude of fracture toughness. The micromechanics investigation found relative motion between fibers and fiber bundles. The high levels of fracture toughness measured were attributed to the ability of all levels of the microstructure to deform, which resulted load sharing that lowered the stress concentration of the crack or notch.

INTRODUCTION

Ceramic matrix composites have been in evolution for many years because they have shown promise as viable materials for structural application in high temperature service. Woven fabric reinforced materials exhibit the best quasi-isotropic strength characteristics, but suffer from interlamellar shear failure. Three dimensional woven reinforcement can defeat the shear failure problem, but lower strength materials are the penalty. The properties most often measured and modeled for these composites have been tensile elastic modulus [1,2], stress-strain [3,4], and tensile failure [5-7], which are the "primary properties." Less studied are the "secondary properties" of creep, fatigue [8] and fracture toughness [9].

The effects of environmental exposure has been studied extensively. The effects of Argon and air or oxygen have been evaluated [10-13], but the environmental effects depend on the details of composite composition and manufacturing method.

The focus of this paper is on the micromechanics of fracture toughness, a material property measured using the concepts of fracture mechanics. Fracture toughness is used in the design of engineering structures, just as are modulus and tensile strength, so it is important that these materials exhibit as high a fracture toughness value as possible. Fracture mechanics was developed for homogeneous solids, so the application of fracture mechanics to inhomogeneous materials carries some risk. In this paper, the micromechanics of fracture toughness are addressed, rather than examination of the validity of applying fracture mechanics concepts, which requires more testing than experimentation.

MATERIALS

The materials evaluated were procured from DuPont-Lanxide Composites Co. of Delaware in 1995. One composite was reinforced by a plain weave (PW) fabric and the other by eight harness satin weave (8HSW) fabric. DuPont-Lanxide Composites is now part of the Allied Signal Co. The dimensions of the PW composite was 75 x 205 mm by 3.4 mm thick, and the 8HSW composite was 115 x 225 mm by 3.2 mm thick. The edges of the composites were parallel to the fabric tow directions.

Fibers in the PW reinforced composite were Ceramic Grade Nicalon. Pyrocarbon was deposited on the fibers as an interface material. Bundles of these fibers were woven into a fabric that was cut and stacked into seven layers. The SiC matrix was emplaced by chemical vapor infiltration (CVI) at 700-1200 °C. The resulting composite contained about 35 vol.% fibers, with a porosity of about 10%, giving a density of 2.3 g/cc [14].

Fibers in the 8HSW reinforced composite were Ceramic Grade Nicalon. The fiber-matrix interface in this composite consisted of two layers, both deposited by CVI. An inner layer of BN was designed to break during material deformation and the outer layer of SiC was designed to protect the fibers during matrix infiltration. The matrix was alumina formed at

900-1100°C by the Dimox process that wicks aluminum metal into the reinforcement and converts it to alumina by the presence of oxygen. The resulting composite contained about 35 vol.% fibers, with a porosity of about 10%, giving a density of 2.3 g/cc [14].

The dimensions of the fabric microstructure are listed in **Table 1**. Fiber size varied by several micrometers, a characteristic commonly reported for Nicalon, but a large percentage of fibers in these composites were about 15 μm in diameter. Approximately 5000 fibers were counted per fiber bundle (tow) in each composite. The cross-sectional dimensions of the fiber bundles depended where in the fabric they were measured, but the bundles were generally flat. Fabric architecture can be described as consisting of repeating units, or "unit cells." The dimensions of the unit cell in each composite was measured. The microstructural information is shown more graphically in some of the illustrations to be used in later sections and in the cross-section of **Fig. 1**.

Table 1
Reinforcing Fabric Microstructural Dimensions

Fiber diameter (approximate, μm): 15
Number of fibers per fiber bundle: 5000
Typical fiber bundle cross sectional dimension (mm): 1.1 x 0.2
Cross-sectional area of fiber bundle (mm^2): 1.4
Packing of fiber bundle (%): 66
Unit Cell size (mm): PW = 3 x 3 mm 8HSW = 9 x 9 mm

The tensile properties of these composites, as listed in company information [13], are shown in Table 2. These properties were not measured as part of the present research.

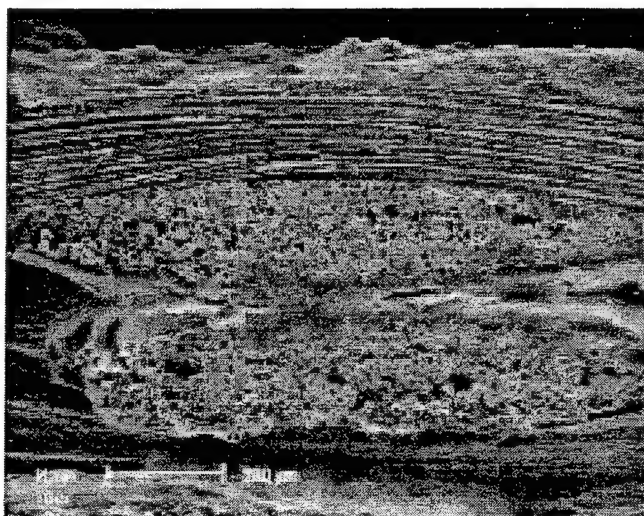


Fig. 1 Cross-sectional view of the PW composite showing the shape of the fiber bundles (tows) and some of the porosity found in the material.

Table 2
Tensile Properties of Composites
(as determined by DuPont-Lanxide)

Temperature	23°C	1100°C
<u>PW Enhanced SiC_f/SiC_m Pyrocarbon interface</u>		
Strength (MPa)	215	212
Elongation (%)	0.41	0.50
Modulus (GPa)	140	114
Proportional Limit (MPa)	53	73
<u>8HSW Ceramic SiC_f/Alumina_m BN/SiC interface</u>		
Strength (MPa)	246	190
Elongation (%)	0.62	0.53
Modulus (GPa)	144	129
Proportional Limit (MPa)	65	66

Specimens

The principal method of investigation was the loading of small compact tension specimens within the scanning electron microscope (SEM) so that the fracture process could be observed using the high resolution and depth of field of that instrument.

All experiments were performed on compact tension (CT) specimens approximately 25 mm square. Pin loading holes approximately 4.76 mm in diameter were cut using diamond encrusted core drills, and the notch was cut using a slow speed diamond encrusted slitting saw. A thick blade (0.5 mm) was used to make most of the cut ($a/w \approx 0.5$), and a thin blade (0.33 mm) was used to produce a sharp notch. The radius of the notch was found to be important to the fracture process, as will be described.

Specimens were cut from the as-received material and slits were made parallel to the sides. Specimens with notches in the two orthogonal directions were cut to test the isotropy of the material.

Pieces of each composite approximately 40 x 120 mm on the side were cut for exposure to 1100°C for 146 hrs. One piece, 40 x 80 mm, was exposed in air and the other piece, 40 x 40 mm, was heated in an alumina tube filled with flowing argon. The oxygen content of the argon was given as not more than 2 ppm by volume [15]. Thus, with these heat treatments, it would be possible to examine the effect of high temperature exposure, with and without an oxidizing atmosphere to determine the effect of each, when compared to the as-received (AR) material.

After exposure to 1100°C, CT specimens were made, and notches were cut as far from the edges as possible, considering that oxygen might have diffused into the edges easier than from the flat surfaces. The end of the notch in each specimen was no closer than about 12 mm from an exposed edge. If oxygen diffused to the notch tip from the edge, the diffusion rate would have exceeded $\approx 2 \times 10^{-8}$ m/sec at 1100°C.

Experimental Procedure

Specimens were loaded to failure both in a laboratory testing machine and

using a loading stage for the SEM [16], all at ambient temperature. The stress intensity factor at failure (fracture toughness) was computed by using the load at fracture in the ASTM formula [17]. Some of the specimens were "dished." The dishing process removed material by abrasion over a surface area approximately 7 mm in diameter by about one layer deep in the area surrounding the notch tip. Dishing allowed access to the fibers and matrix beneath the surface of the composite. Comparative experiments were conducted between dished and undished specimens, and it was concluded that the dishing had very little effect except to reduce the specimen thickness.

First, several specimens were broken in the laboratory machine so that an estimate of fracture toughness was obtained. Subsequent specimens were load cycled between 10% and 90% of the fracture stress intensity for 100,000 to 200,000 cycles to start a crack. In most cases, a crack of less than 1 mm was found growing from the notch, at least in the surface layer of the composites. If the notch tip was sharp ($\approx 50 \mu\text{m}$ radius), only one crack was found. If the notch tip was blunt, then multiple cracks were likely. Since it was not possible to determine whether observed cracks went through several layers, the notch length was used in the fracture toughness calculation. In all cases, cracks were short. Also, these materials exhibited either no crack growth, or very little, before fracture.

During experiments in the SEM, photographs were made at various levels as load was increased to fracture. It was frequently possible to obtain photographs within a few Newtons of the fast fracture level. The appropriate magnifications for examination of these materials were 25 to 50X because of the macroscale of the fabric reinforcement. The stereoimaging technique [18] was used to examine the photographs for artifacts and to visualize the displacements caused by loading. The automated photocomparison system, DISMAP [19], was used to measure displacements from some of the photographs.

After specimen fracture, the level of fiber pull-out was examined directly in the SEM, and observation of the fibers was made at high resolution to examine the interfaces and determine the extent and thickness of interface layer and matrix adhesion.

RESULTS

Fracture Toughness

Composite fracture characteristics were examined on several levels. From maximum load and notch length, the fracture toughness was calculated, as listed in **Table 3**.

Table 3
Allied Signal (formerly DuPont-Lanxide) Composites Evaluated

Specimen Number	Condition	Fracture Toughness MPa√m	Notes	Analysis Data Set
<u>8HSW Nicalon Fibers - Alumina matrix SiC_f/Al₂O₃_m</u>				
601	As-received	.-	Blunt notch; Failed in pin hole	
604	As-received	22.4	Dished	1296
605	1100°C Air	14.7	Blunt notch	
606	1100°C Air	> 13.8	Not broken	
609	1100°C Air	17.5	Sharp notch	
610	1100°C Air	18.9	Dished	
611	1100°C Air	20.5	Dished	1345
621	1100°C Argon	20.0	Sharp notch	1346, 1347
623	1100°C Argon	17.7	Sharp notch, dished	1348, 1349 1351, 1352
627	As-received	26.8	Sharp notch	
<u>PW Nicalon fibers - Silicon Carbide matrix SiC_f/SiC_m</u>				
607	1100°C Air	11.8	Blunt notch	
608	1100°C Air	12.8		1297
615	1100°C Air	10.0	Sharp notch	
617	1100°C Argon	10.8	Sharp notch	
622	1100°C Argon	10.0	Dished	1344
624	1100°C Air	12.2	Dished	
625	As-received	12.7	Dished	1343
626	As-received	13.4	Sharp notch	1353, 1354
628	As-received	13.4	Notch 45° to weave axis.	

The cracks that had grown a little ($< 50 \mu\text{m}$) during loading from the notch tips in some of the specimens were not considered in the calculation because it is unlikely that they existed through the specimen thickness.

Fracture toughness results are graphed in **Figs. 2 and 3**. For the PW reinforced material, fracture toughness was typified as being variable, but for the 8HSW reinforced composite, the fracture toughness was more repeatable. The variability of fracture toughness in the PW makes it difficult to determine with certainty if the exposure at high temperature had much effect, while for the 8HSW material, it is easier to conclude that the exposure did have an effect, but that the environment was less important than the temperature. For both materials, more data are needed to clarify the effects of temperature and environment.

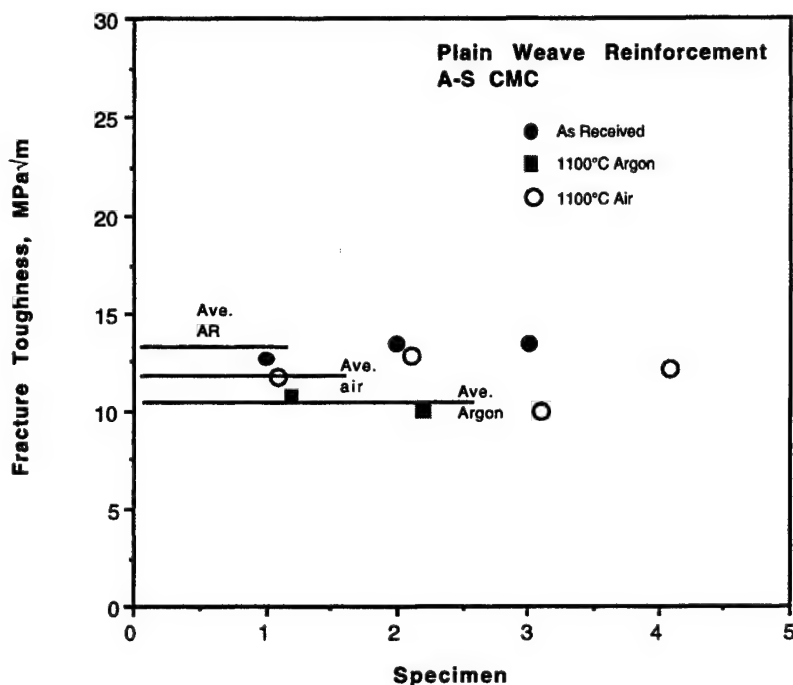


Fig. 2 The effect of 1100°C exposure to Argon and air on the fracture toughness of the PW/SiC composite. The environmental effect, if any, is small.

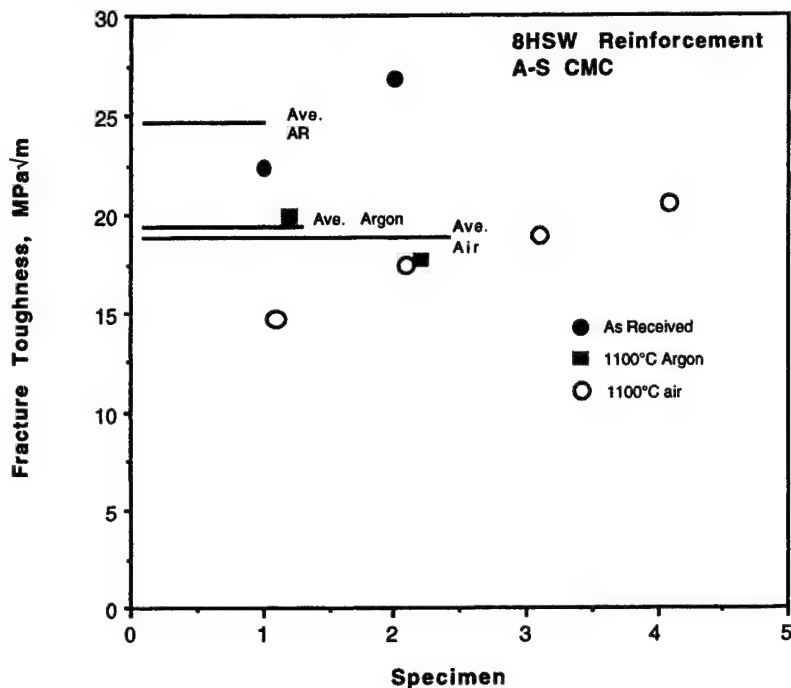


Fig. 3 The effect of 1100°C exposure to Argon and air on the fracture toughness of the 8HSW/alumina composite. There is an effect of high temperature exposure, but no effect of environment is evident.

Micromechanics Analysis

The main task of this research was micromechanics analysis of the fracture process. Photographs were made as a function of increasing load during the fracture of specimens within SEM using the loading stage. Displacements were measured from these photographs using the DISMAP system; the analyses are identified in Table 3. Displacements were measured by DISMAP at nodes on a square grid of finite dimension, while the photographs can be stereoimaged with the eyes on a continual basis. Thus, displacements can quantify only part of what the visual system can perceive.

Strains were computed from displacements by the stereoimaging

technique [18]. The strain calculation makes the assumption that the material is acting as a continuum, which is only partially correct for these composites. Individual fibers and fiber groups within bundles can be observed by stereoimaging to be moving relative to other fibers and groups of fibers. This deformation is captured in the analyses as shear strains.

The magnifications of the photographs from which displacements were measured were 25 and 50 times, as required to obtain deformation information on the scale of the microstructure. However, these magnifications were not high enough to reveal many of the microcracks that had formed. Where detected, cracking was accounted for in the strain computations. However, large strains at some locations may, in fact, be due to undetected crack formation.

Two examples each from the PW and the 8HSW composites have been selected to illustrate the behavior observed. Other, similar analyses are shown in the Appendix. There is not an equal weight on each material and environment because the experimental results were not of equal quality. Some experimental results were better suited for analysis than others.

Each analysis shows Mohrs circles of strain and the various regions of the microstructure. Mohrs circles show the magnitude of the maximum shear strain and the magnitude of the coordinate strains relative to shear by the direction of the line through the circle. The direction of load application was horizontal in each of the illustrations, and if the deformation was mostly tensile, then the line is also approximately horizontal. When the line through the Mohrs circle is nearly vertical, it is an indication that the shear strain was large relative to the axial strain.

Dotted lines separate regions of fiber bundles in the two directions and show regions of matrix. Regions of matrix only, without visible fibers, are labeled "m." The directions of fibers within bundles are shown as parallel lines between the Mohrs circles. Voids within the material are noted as "VOID." Cracks usually originate from the notch, drawn in white in each illustration, unless the region of analysis was sufficiently far ahead of the notch that it was not visible.

In the first illustration, **Fig. 4**, a 8HSW/alumina specimen has cracked at the notch tip and torn across the first fiber bundle to the first transverse oriented fiber bundle where an additional crack formed in the loading direction. The maximum shear strains are found in the tearing fiber bundle near the notch, at the crack tip, and around the voids at various locations. Many of the large strains are principally shear. Most of the strains in the torn fiber bundle between the notch and the crack tip are, in fact, fibers and groups of fibers shearing relative to one another.

Cracking in a transverse fiber bundle is shown in **Fig. 5** in a 8HSW/alumina specimen. The notch that caused the stress concentration was ≈ 0.5 mm above the top of the area shown. Regions of high strain can be seen near the boundary of the transverse and longitudinal fiber bundles on the right and in the lower left where fibers disappear beneath a region of matrix. On the right, the strains are predominately in the direction of loading (horizontal), while at the fiber bundle/matrix boundary, the strains are mainly compressive. Strains at microstructural transitions that are larger than those at the crack tip may indicate that the crack seen is superficial, i.e., does not penetrate very deep into the structure.

The microstructure and the material response of the PW/SiC composite illustrated in **Fig. 6** is complex. The microstructure is revealed at several levels in this specimen due to "dishing." The crack is growing in a region where parts of fibers in both directions may be seen, and matrix regions and voids are found in the regions where fiber directions are changing. The maximum shear strains are found in the regions around the voids, near the crack tip, and at some locations where fiber directions are changing.

A similar illustration of microstructural response is shown in **Fig. 7**, a PW/SiC specimen that was also dished. In this case, cracks were found in the lower left near the large void and in the lower right where a fiber tow is separating from a matrix region. No (known) crack has formed at the notch tip. The largest strains are dominated by shear and are found near voids, in the transition regions between fiber bundle edges, and near the cracks tips.

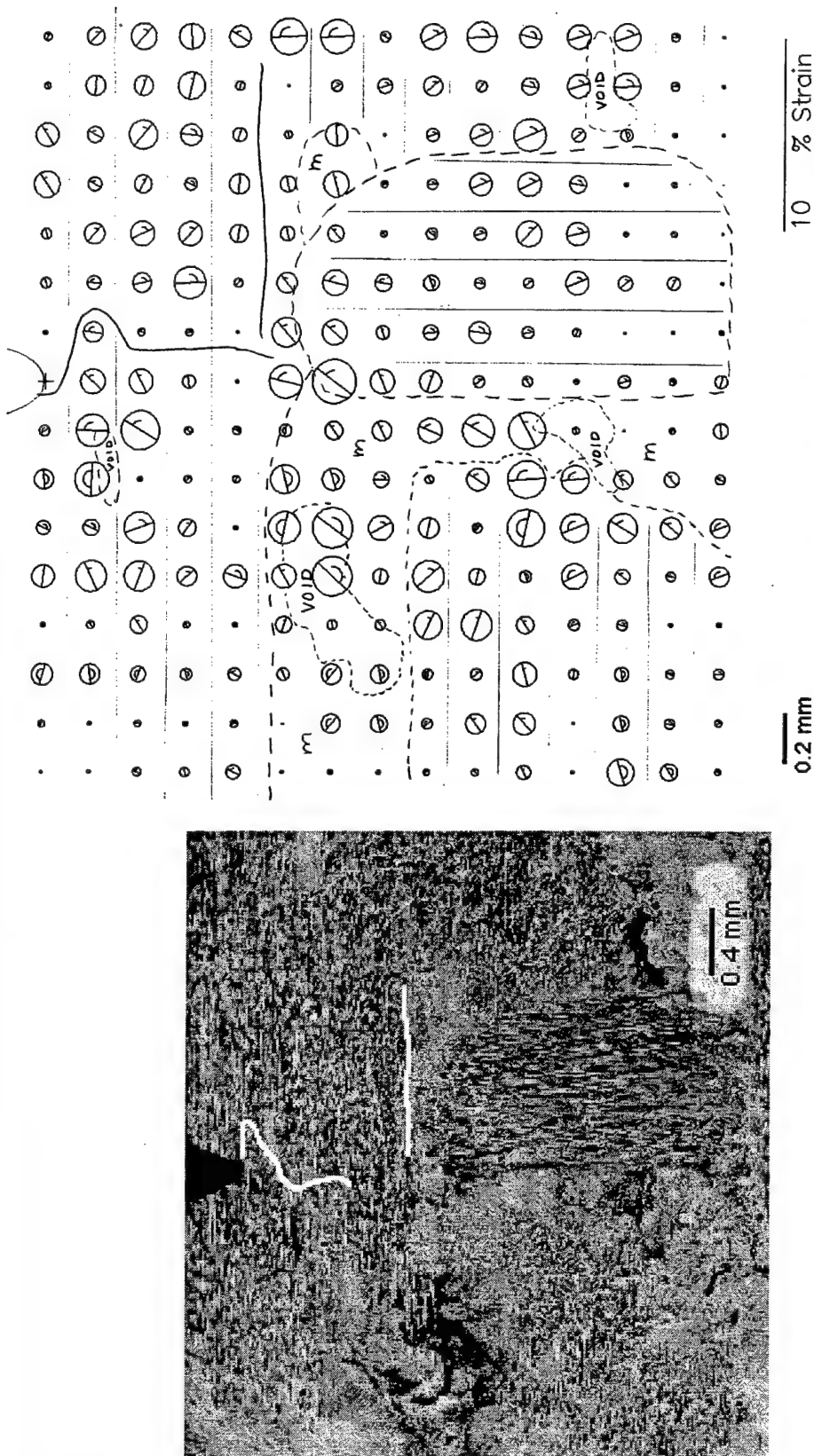


Fig. 4 8HSW/alumina specimen exposed to 1100°C for 146 hrs. in Argon.

The analysis was done at $K = 13.6 \text{ MPa}\sqrt{\text{m}}$, 77% of $K_c = 17.7 \text{ MPa}\sqrt{\text{m}}$.

Left: Region analyzed. Right: Mohr's circles of strain with the edges of the microstructural features shown as dotted lines.

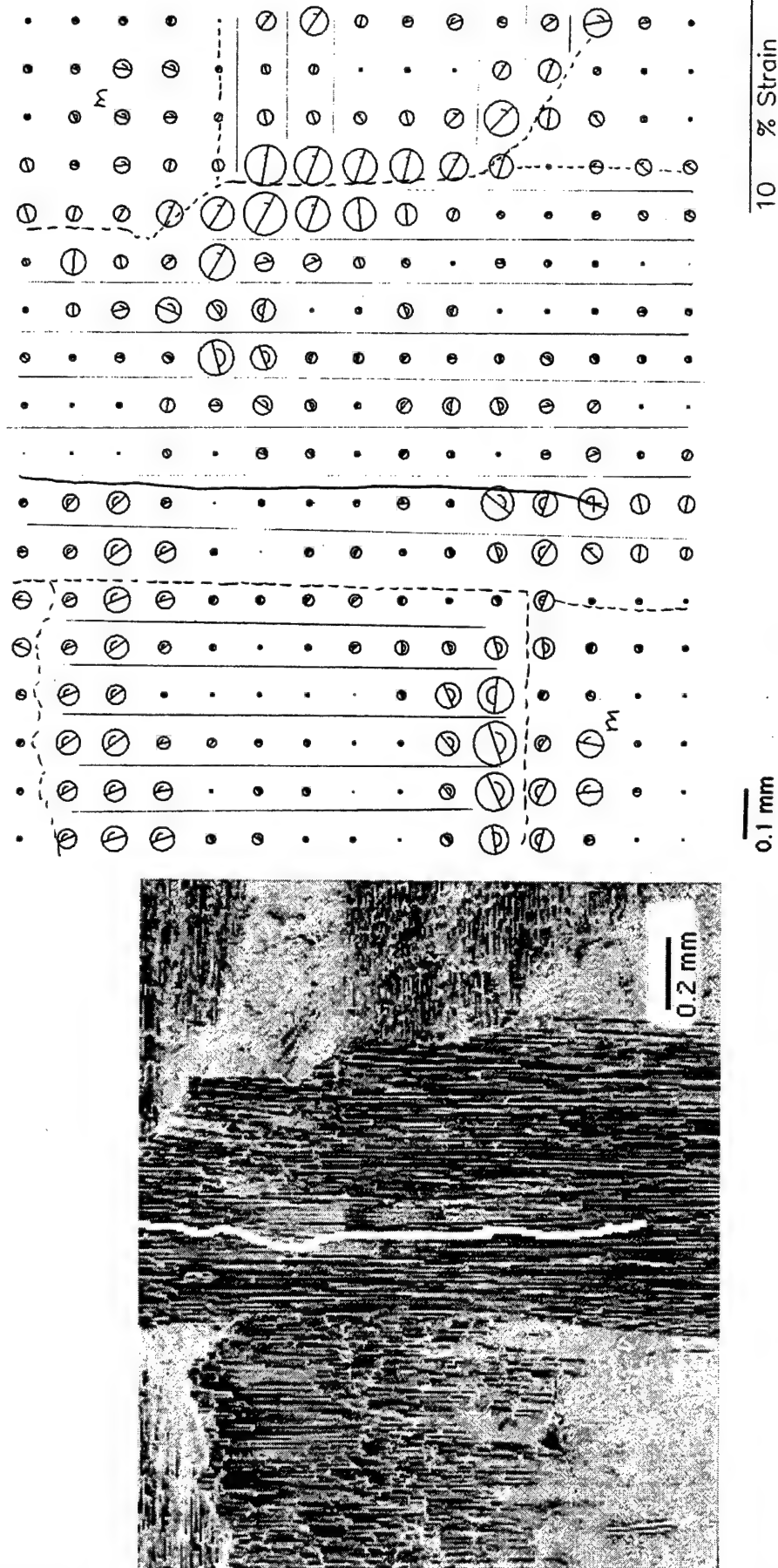


Fig. 5 8HSW/alumina specimen exposed to 1100°C for 146 hrs. in air. The analysis was done at $K = 12.1 \text{ MPa}\sqrt{\text{m}}$, or 83% of $K_c = 14.6 \text{ MPa}\sqrt{\text{m}}$. Left: Region analyzed. Notch is approximately 0.5 mm above the top of the photograph. The crack is shown in white. Right: Mohr's circles of strain with the edges of microstructural features shown as dotted lines.

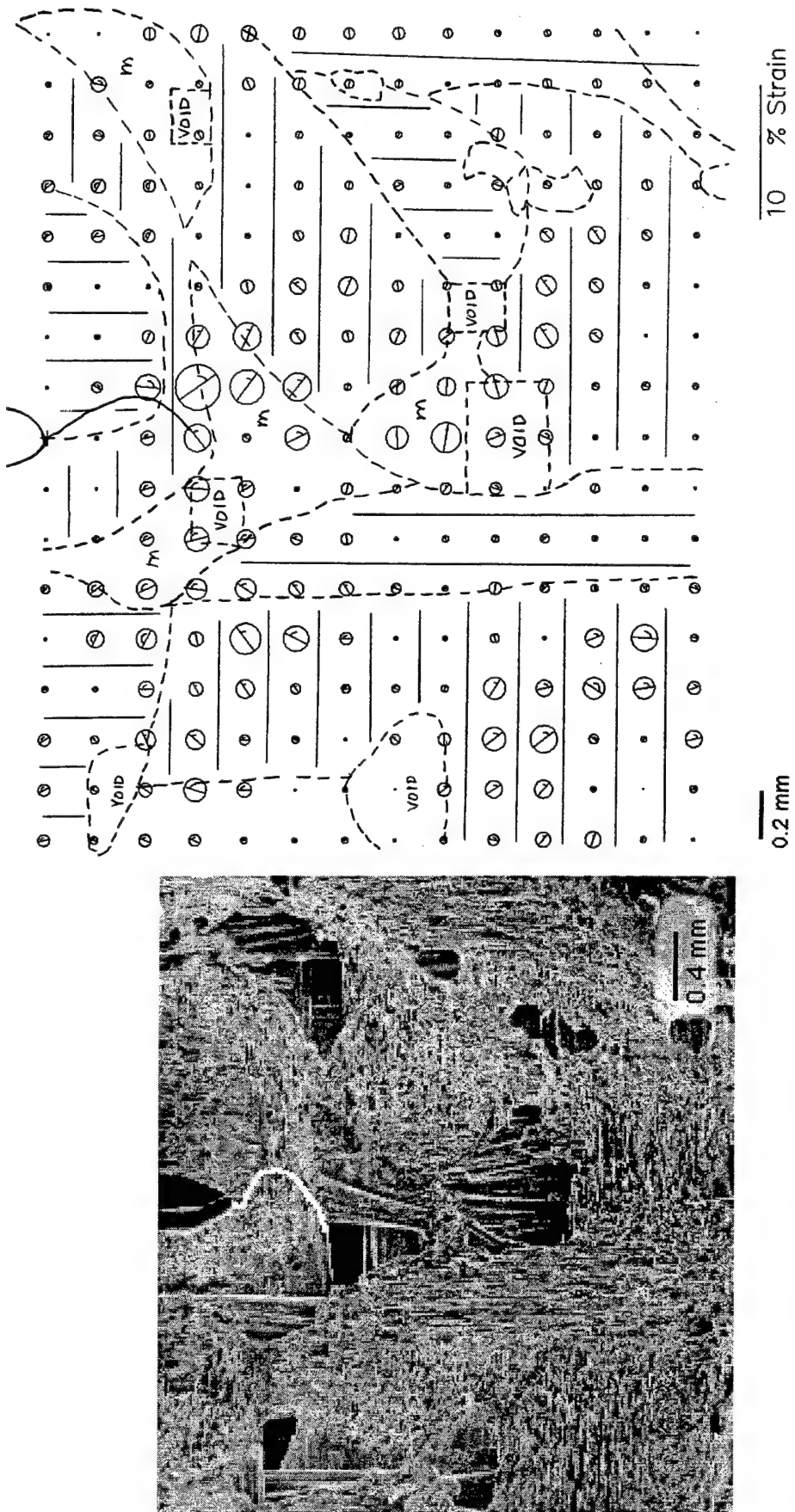


Fig. 6 PW/SiC specimen As-received. Analysis at $K = 12.0 \text{ MPa}\sqrt{\text{m}}$, 94% of $K_c = 12.7 \text{ MPa}\sqrt{\text{m}}$. Left: Region analyzed. Right: Mohr's circles of strain with edges of the microstructural features shown.

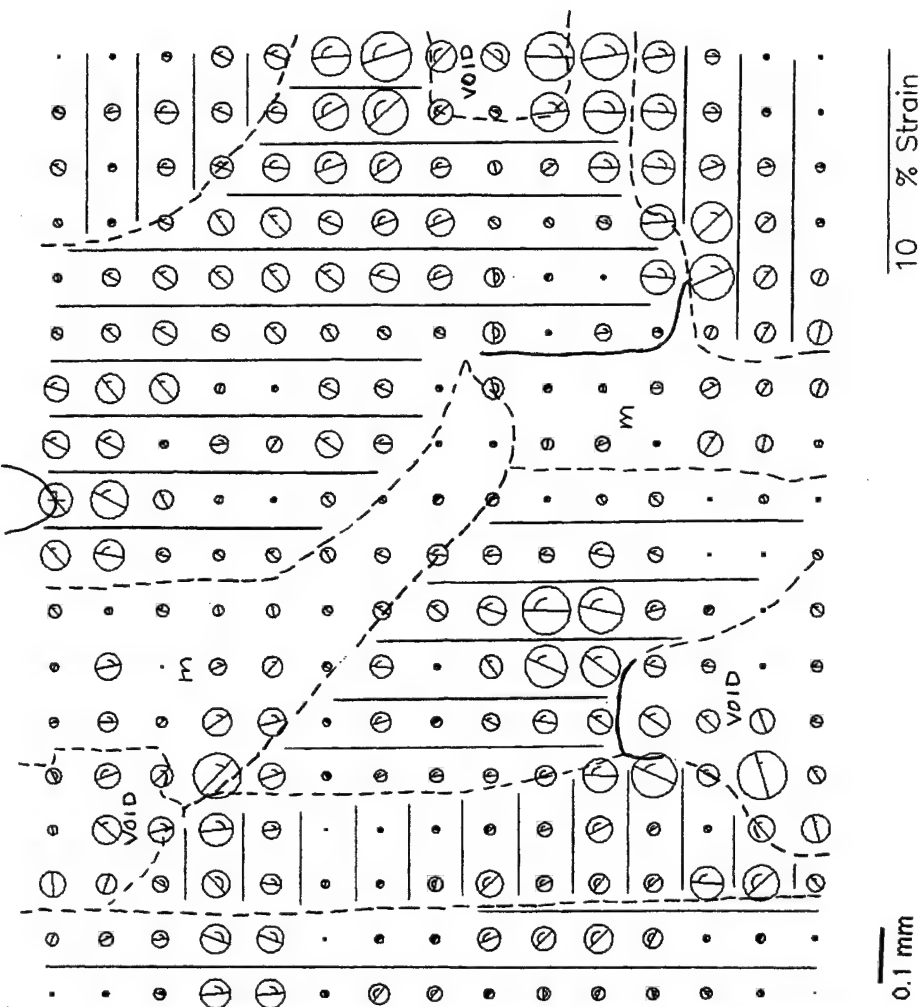


Fig. 7 PW/SiC specimen exposed to 1100°C for 146 hrs. in Argon. The analysis was done at $K = 9 \text{ MPa}\sqrt{\text{m}}$, or 90% of $K_c = 10.0 \text{ MPa}\sqrt{\text{m}}$. Left: Region analyzed. Right: Mohr's circles of strain with the edges of microstructural features shown as dotted lines. Two cracks in the structure are shown. Notch is at the top.

Summary of Micromechanics Analyses

The deformation analyses of Figs. 4 -7, as well as in the additional analyses presented in the Appendix, exhibit some common features. Strain concentrates in the following locations:

- (a) near voids caused by incomplete matrix infiltration,
- (b) near crack tips, and
- (c) near fiber bundle edges, especially where the bundles cross one another in the weave.

Large strains near a void (a) is especially well illustrated in Figs. 4 and 6. Large strains at crack tips (b) are shown in all the figures, while large strains at fiber bundle edges and crossings (c) are the most obvious in Figs. 5 and 7.

Maximum effective strains at crack tips are determined as 0.010 to 0.034, while at voids the range is 0.013 to 0.034, and at boundaries the values are up to 0.14. In the fiber bundles, the maximum effective strains are about 0.10 in the regions away from boundaries.

Fractography

At the end of each experiment in the SEM, the specimen was broken, but the two halves were not completely separated. Many fibers did not break along the primary crack line; fracture tens of micrometers away from the fracture surface was common, with subsequent pull-out of parts of fiber bundles and individual fibers from the bundle. This general observation is illustrated in **Fig. 8**, which shows the fracture of a PW/SiC specimen.

Fibers pulled out were examined at about 200X to determine the length of the pull-out, and at relatively high resolution, 1000 to 2000X, to see if coating remnants and matrix could be found on them. In some cases, porosity in the matrix was found and examined. Some of the fibers so examined are shown in following figures. **Fig. 9** is a detail of the fracture shown in **Fig. 8** of As-received PW/SiC.

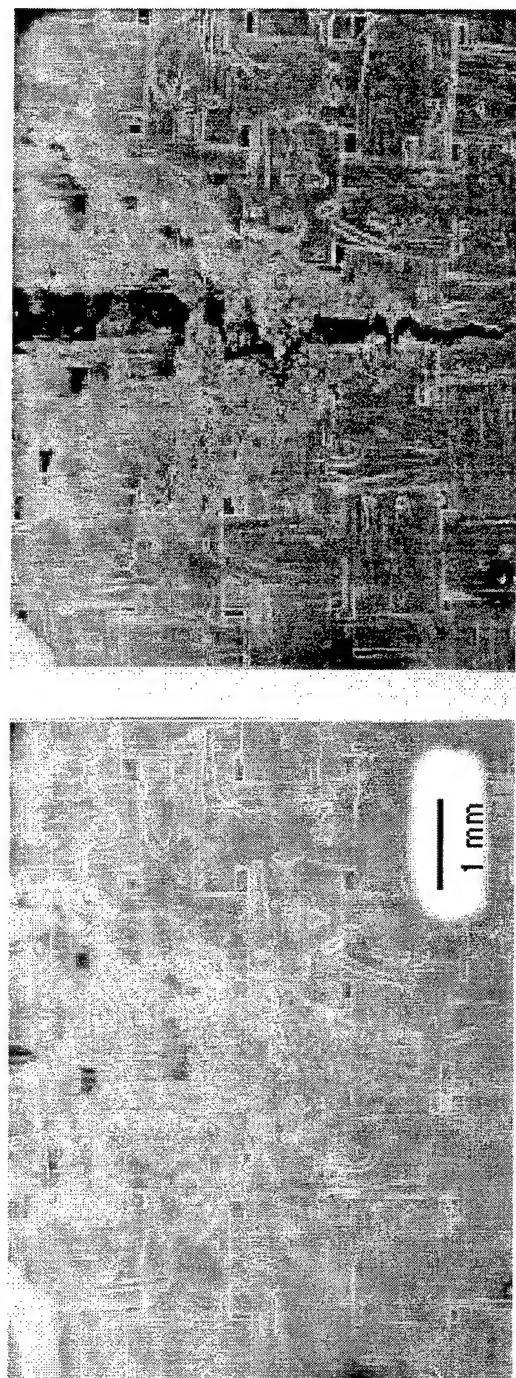


Fig. 8 PW/SiC specimen As-received that was dished. The level of voids on the interior of the specimen may be seen on the left, before fracture. After fracture, on the right, may be seen the fiber pull-out lengths - between a half and one mm.

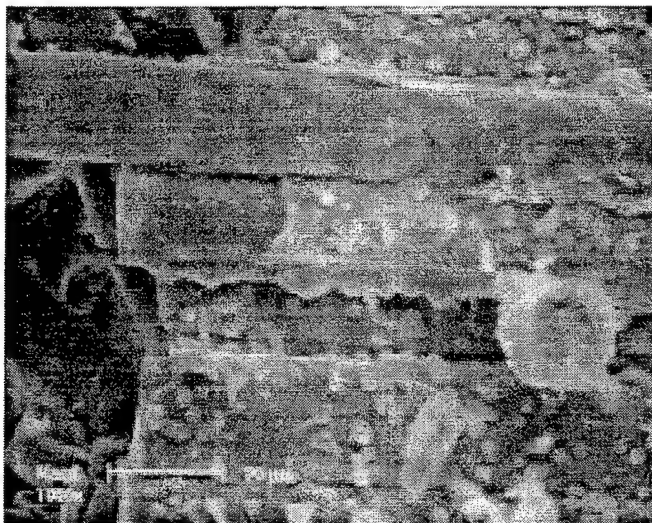
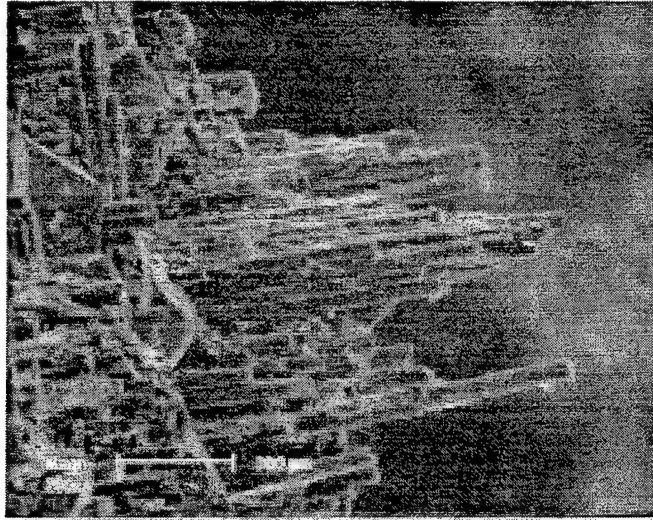


Fig. 9 This is a detail of Fig. 8. The top fiber shows coating that has been partly removed during fracture. The fiber below shows matrix partially broken away that is dotted with particles.

The above fracture surfaces may be compared to those in **Fig. 10**. The fiber coating adhering to the fiber in this sample, exposed to 1100°C, may be thicker than that found in the As-received material, but not by very much. Otherwise, there seems to be very little difference. There is some fiber pull-out, but only about 100 μm , indicating the interface strength is not too strong, and has been controlled by the fiber coating.

One of the 8HSW/alumina specimens fractured is shown in **Fig. 11**. The pull-out distances for this composite may be somewhat greater than for the PW/SiC composite, although that was not examined statistically, and less debris was found on the fracture surfaces than was found on those of the PW/SiC composite. Coating was found adhering to the fibers in some locations.

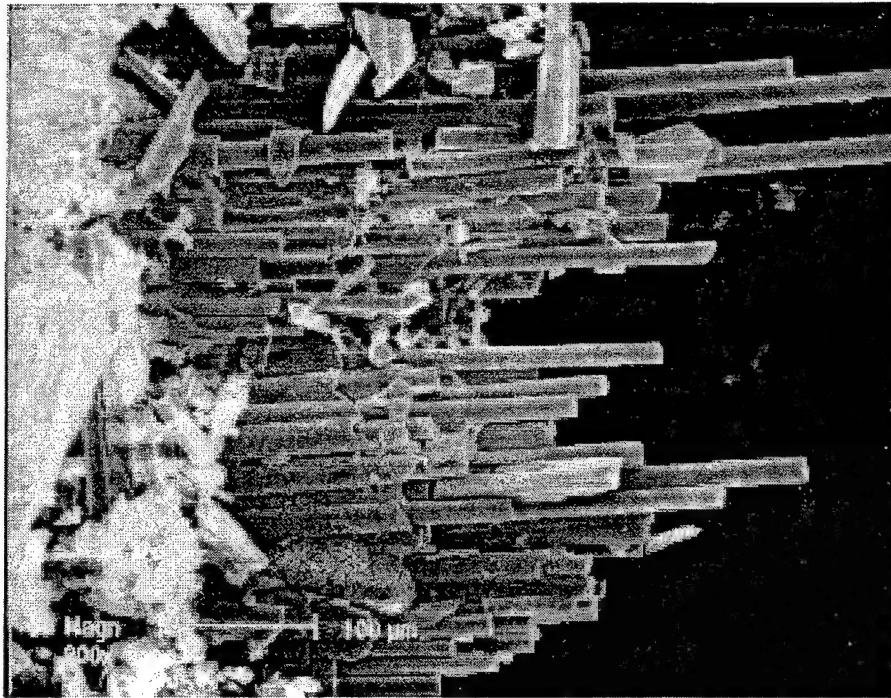


(a)

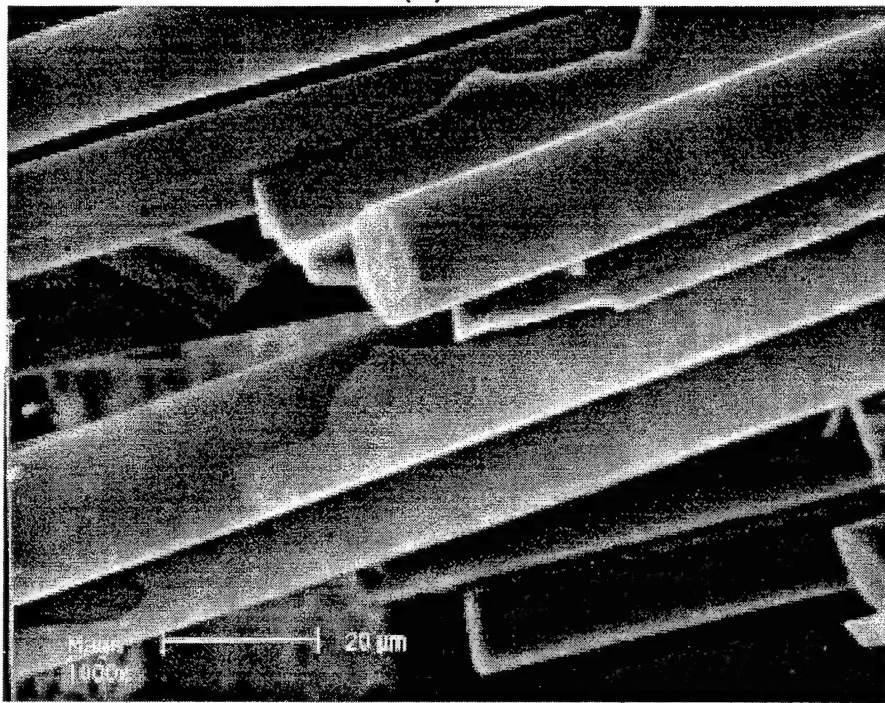


(b)

Fig. 10 Fracture of PW/SiC specimen exposed to 1100°C for 146 hrs. in Argon. (a) Fiber bundle pull-out of 100 to 200 μm ; (b) Detail of the adherence and fracture of the coating seen on the central fiber. Note also the large amount of debris from the matrix that adheres to the fibers.



(a)



(b)

Fig.11(b) Fractography of 8HSW/Alumina specimen exposed to 1100°C for 146 hrs. in Argon. (a) Fiber pull-out of $\approx 200 \mu\text{m}$; (b) Note the partial coverage of the central fibers by coating.

In general, the length of the pulled-out fibers appeared to be independent of weave and heat treatment, which is not to indicate that they were all the same, only that they were not systematically related to microstructure or environmental exposure. A quantitative study of fiber pull-out length was not made because of the small differences found.

DISCUSSION

The magnitude of the strains determined was less than about 0.03, and was much less than that in most locations. Voids in the matrix, fiber bundle directional transitions, and crack tips were the locations of maximum strains. Thus, relatively large strains are dispersed at locations other than the crack tip, and this gives the appearance of a large "plastic zone" surrounding the notch, or crack tip. Thus, all the deformation associated with fracture does not occur at the stress concentration of the crack tip, but is spread through out a "process zone," or "plastic zone," as is found in metallic specimens that demonstrate fracture toughness values $> 10 \text{ MPa}\sqrt{\text{m}}$.

Deformation within a crack tip plastic zone in metals results from dislocations that are emitted and move away from the crack tip. Deformation in these ceramic matrix composites results from fibers and fiber bundles move relative to one another in the region of stress concentration (notch and crack tip). The effect is the same in the two types of structures. In the metal, dislocation generation and motion lowers the crack tip stress concentration, while in these composites the fibers and fiber bundles sliding relative to one another allow load sharing between fibers and bundles, thereby lowering the stress concentration caused by the notch and crack.

Conventional wisdom portrays the interface between the fibers and the matrix as being of paramount importance in the failure process. coatings are applied to fibers to create a weak interface that will break under stress, thus allowing the fibers to move relative to one another. While the fiber/matrix interface is important, this research has determined that it is not a complete description of the importance of fiber/matrix interaction during fracture.

The matrices of these composites are described as "silicon carbide" and "alumina" which is mainly a description of their composition. The mechanical properties of the matrices of these composites were measured by mechanical microprobe (nanoindenter) and it was found that the modulus and hardness of each was much lower than would be expected based on the properties of the bulk ceramics with the same general composition [20]. The measured values are summarized in **Table 4**.

Table 4
Matrix mechanical properties

Composite	Modulus	Hardness
Fiber weave/matrix	GPa	GPa
<u>As Received</u>		
8HSW/alumina matrix	150	5.8
PW/silicon carbide	51	3.3
<u>After exposure to 750°C for 64 hrs.</u>		
8HSW/alumina matrix	123	3.8
PW/silicon carbide	57	13.3
<u>Bulk Ceramics (for comparison)</u>		
Alumina	386	15
Silicon carbide	390	24

As seen in this table, the matrices of these composites are compliant and soft when compared to bulk materials; for alumina, E and H are about 40% of the bulk, and for SiC, E and H are only about 15% of the bulk. The result of this high compliance is that fiber bundles should be able to move relative to one another in the stress field of a crack tip and share the load, and that is what micromechanics analysis has found experimentally.

The combination of matrix characteristics and micromechanics measurements leads to the conclusion that the relatively high fracture toughness of these composites is the result not only of fiber coatings that can be broken in the high stress field of a notch or crack, but is also attributed to the low compliance of the matrix that allows fibers and

fiber bundles to share load. The regions of lowest compliance, the voids, also contribute strongly to fiber bundle movement and load sharing.

CMCs with porous matrices were modeled by Tu, et al. [5], who predicted that strong interfaces between matrix and fibers would produce a composite with high fracture toughness if the matrix was porous. The result of porosity would be to lower the modulus. Since the measured moduli of the composites investigated here is low, compared to bulk properties, it was thought that this theory would perhaps be applicable. However, the theory indicates that a much larger change than was measured would be required to significantly alter fracture toughness.

The effect of environment on fracture was caused probably by a decrease in fiber strength caused by exposure to 1100°C. Micromechanics analysis did not show any result that could be attributed to exposure in air or Argon at 1100°C. Fractographic analysis also showed no features attributable to exposure to air, Argon, or to high temperature. Since the fracture toughness was lowered about the same amount by exposure to both air and Argon, it is concluded that the exposure to high temperature caused the drop in toughness, not the environment of the exposure. Thus, it is presumed that the fiber strengths were lowered by exposure to 1100°C, and that this effect was greater than any change caused by the chemical nature of the environment.

Data on the strengths of fibers and fiber bundles and their degradation by high temperature exposure exists [21,22]. It is known that these fibers contain oxygen and free carbon, and the work of Chollon, et al. [23] showed that fibers loose strength after exposure for 1200-1400°C in high purity Argon for 1 hr. The strength reduction was attributed to the coarsening of the SiC grains in the fiber or the effects of free carbon and oxygen. The kinetics of the processes of fiber strength reduction are very sensitive to temperature, the details of fiber manufacture, and the effects of fiber coating, so whether or not sufficient degradation occurred from 1100°C exposure for 146 hrs. for the fibers in these composites is not known, but it is likely that strength was degraded and that this was the cause of fracture toughness reduction.

CONCLUSIONS

1. This research has found that the ability of fibers and fiber bundles to move relative to one another contributes to the fracture toughness of CMCs. Stresses are lowered within the elevated stress field of a crack or notch because these microstructural elements can share the load. The fracture toughness of fabric without matrix is elevated for the same reasons. Fiber and fiber bundle motion is controlled by the characteristics of the weave, the mechanical properties of the matrix, and the level of voids within the composite.
2. High fracture toughness is developed in CMCs by : (1) using fibers with high fracture strength, and (2) controlling the strength of the interface between fiber and matrix, usually with coatings, (3) providing a matrix that is relatively low in fracture strength and is compliant, and (4) providing numerous spaces within the CMC that are unoccupied by matrix (voids).
3. Fracture toughness of the composites investigated was relatively high because the fibers were strong, the coatings used gave appropriate levels of interfacial strength, the matrix was compliant, and the volume fraction of voids was relatively large.
4. High temperature exposure probably lowered the strength of the fibers, which reduced fracture toughness. No differences in the micromechanics of fracture that were caused by high temperature exposure in air or Argon were found.

ACKNOWLEDGEMENT

This research was funded by The Office of Naval Research, Dr. Steven Fishman project monitor, Contract N00014-96-C-0076. Byron Chapa, and Jim Spencer provided extensive and able experimental assistance to this research.

REFERENCES

1. M. Ito and T-W. Chou, "Elastic moduli and stress field of plain-weave composites under tensile loading," Comp. Sci. & Tech., 1997, v. 57, pp. 787-800.
2. B. Sankar and V. Marrey, "A unit cell model of textile composite beams for predicting stiffness properties," Comp. Sci. & Tech., 1993, v. 49, pp. 61-69.
3. L. Guillaumat and J. Lamon, "Model of the non-linear stress-strain behavior of a 2D-SiC/SiC ceramic matrix composite (CMC)," in **High-Temperature Ceramic-Matrix Composites I**, A.G. Evans and R. Naslain, eds., *Ceramic Transactions*, v. 57, Am. Ceramic Soc., Westerville, OH, 1995, pp. 215-226.
4. T-S. Chou and P.G. Karandikar, "Damage processes and non-linearity in ceramic matrix composites," *ibid.*, pp. 107-113.
5. W.-C. Tu, F.E. Lange and A.G. Evans, "Concept for a damage-tolerant ceramic composite with 'strong' interfaces," J. Am. Ceram. Soc., 1996, v. 79, pp. 417-424.
6. W.P. Keith and K.T. Kedward, "Notched strength of ceramic-matrix composites," Comp. Sci. & Tech., 1997, v. 57, pp. 631-635.
7. L. Hahn, F. Ansorge and A. Bruckner-Foit, "Damage and failure behavior of a woven C/SiC material," J. Mat. Sci., 1997, v. 32, pp. 5467-5475.
8. A. Dalmaz, P. Reynaud, D. Rouby, G. Fantozzi and F. Abbe, "Mechanical behavior and damage development during cyclic fatigue at high temperature of a 2.5D carbon/SiC composite," Comp. Sci. & Tech., 1998, v. 58, pp. 693-699.
9. K. Goto and Y. Kagawa, "Fracture behaviour and toughness of a plane-woven SiC fiber-reinforced SiC matrix composite," Mat. Sci. Eng., 1996, v. A211, pp. 72-81.

10. F. Heredia, J. McNulty, F. Zok and A. Evans, "Oxygen embrittlement probe for ceramic matrix composites," J. Am. Ceram. Soc., 1995, v. 78, pp. 2097-2100.
11. A. Bandyopadhyay and P. Aswath, "Interfacial stability oxygen response and mechanical properties of a Nicalon fiber reinforced chemical bonded ceramic matrix composite," J. Mat. Sci., 1994, v. 29, pp. 4205-4215.
12. R. Jones, C. Henager and C. Windisch, "High temperature corrosion and crack growth of SiC-SiC at variable oxygen partial pressures," Mat. Sci. & Eng., 1995, v. A 198, pp. 103-112.
13. M. Bouchetou, T. Cutard, M. Huger, D. Fargot and C. Gaul, "Effect of environment on CMCs," in **High-Temperature Ceramic-Matrix Composites I**, A.G. Evans and R. Naslain, eds., Ceramic Transactions, v. 57, Am. Ceramic Soc., Westerville, OH, 1995, pp. 215-226.
14. www.dlcomposites.com: Internet web site for DuPont-Lanxide composites.
15. Industrial grade Argon, Praxair Co., Austin, TX, 512/389-2323.
16. D.L. Davidson and A. Nagy "A low frequency cyclic loading stage for the SEM," J. Phys. E, 1978, v. 11, pp. 207-210.
17. ASTM Standard E399, Am. Soc. Testing and Materials.
18. D.R. Williams, D.L. Davidson and J. Lankford, "Fatigue crack tip plastic trains by the stereoimaging technique," Experimental Mechanics, 1980, v. 20, pp. 134-139.
19. E.A. Franke, D. Wenzel, and D.L. Davidson, "Measurement of microdisplacements by machine vision photogrammetry (DISMAP)," Rev. of Scientific Instruments, 1991, v. 62, pp. 81-91.

20. G. Pharr and D.L. Davidson, "Matrix Properties of Textile Reinforced Ceramic Matrix Composites as Measured by Mechanical Microprobe" (in preparation for Journal of Composites), 1999.
21. M.H. Berger, N. Hochet and A.R. Bunsell, "Microstructure and thermo-mechanical stability of a low-oxygen Nicalon fiber," J. of Microscopy, 1995, v. 177, pp. 230-241.
22. G. Emig and R. Wirth, "Tensile strength of silicon carbide fiber bundles at elevated temperatures," J. of Mat. Sci., 1995, v. 30, pp. 5813-5818.
23. G. Chollon, R. Pailler, R. Naslain and P. Olry, "Correlation between microstructure and mechanical behavior at high temperatures of a SiC fiber with low oxygen content (Hi-Nicalon)," J. Mat. Sci., 1997, v. 32, pp. 1133-1147.

APPENDIX

Seven additional micromechanics analyses of composite fracture are given to supplement those shown in the text.

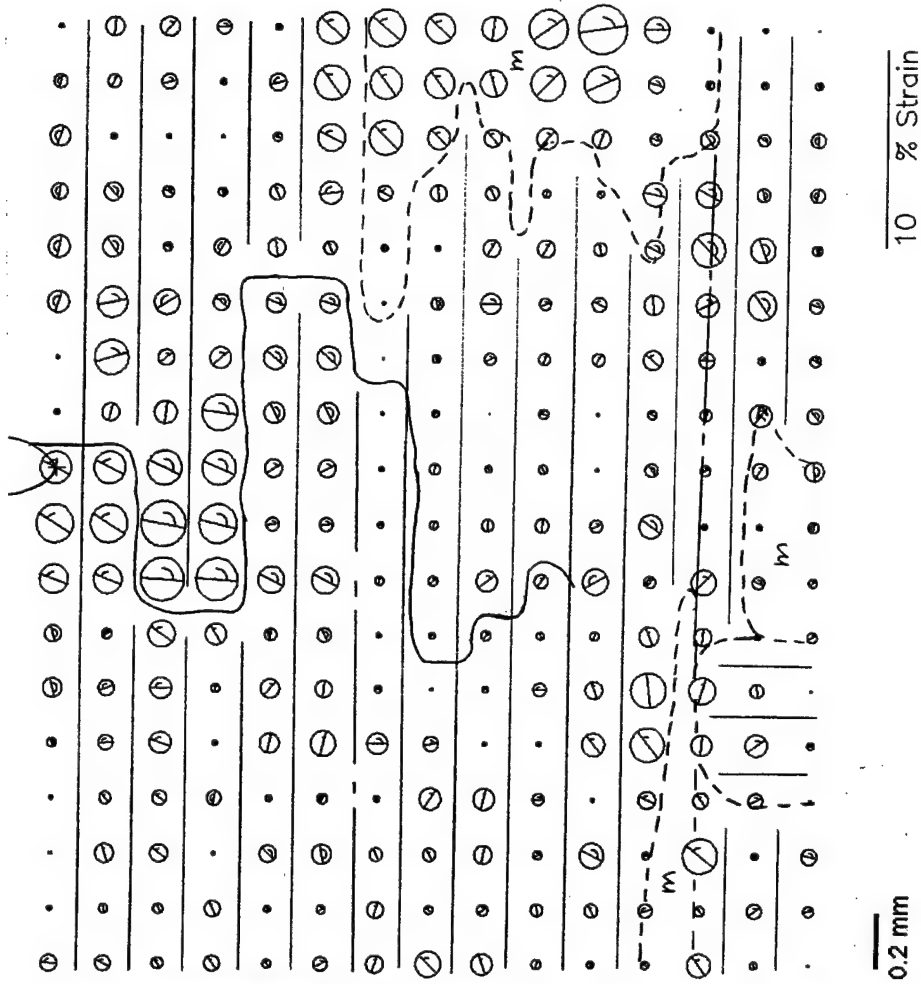
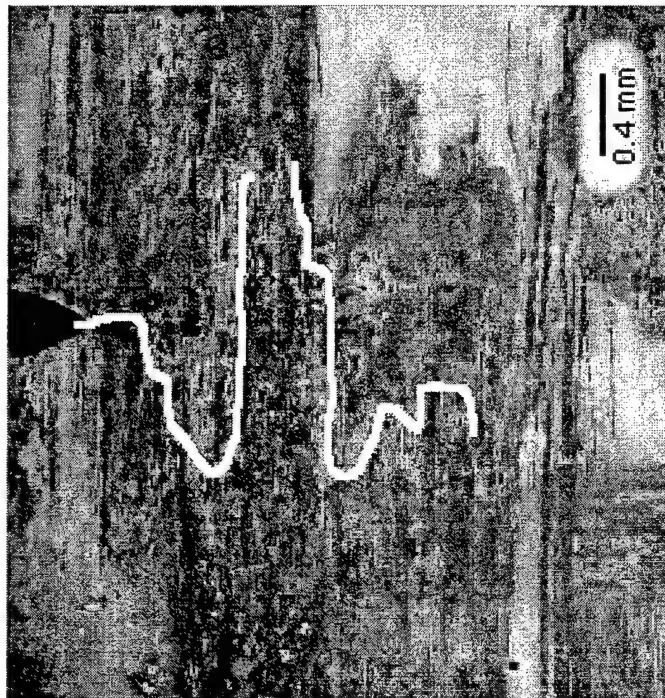


Fig. A1 8HSW/alumina specimen exposed to 1100°C for 146 hrs. in Argon. Analysis was made at $K = 16.2 \text{ MPa}\sqrt{\text{m}}$, or 81% of $K_c = 20 \text{ MPa}\sqrt{\text{m}}$. Left: Region analyzed. Crack is shown in white. Right: Mohr's circles of strain with edges of microstructural features shown as dotted lines.

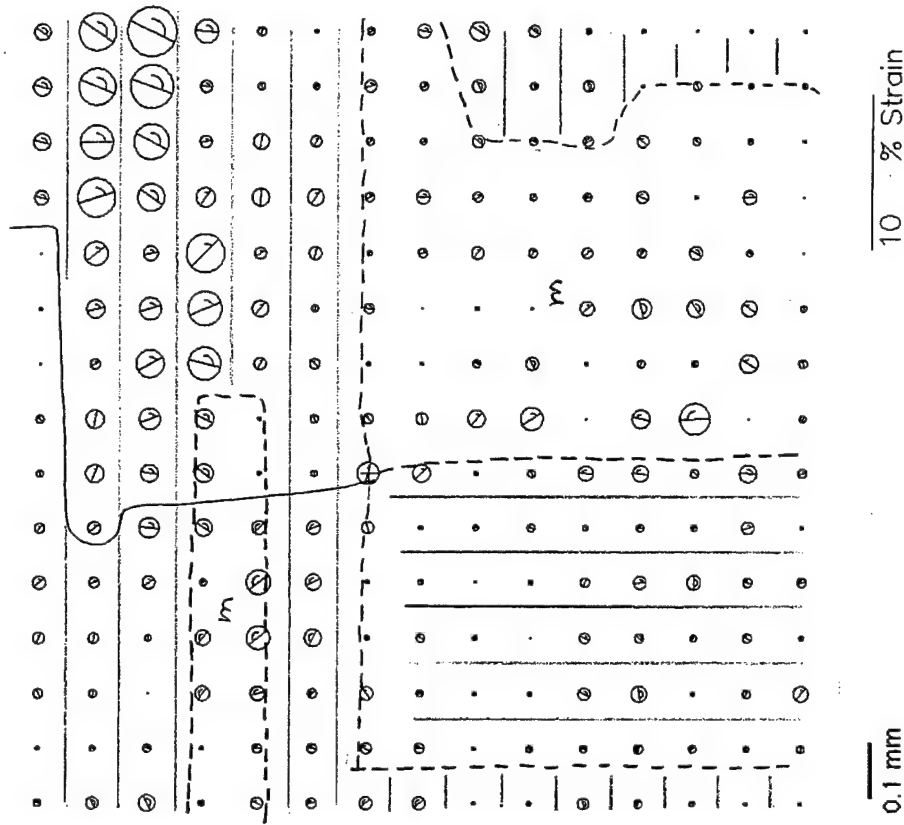
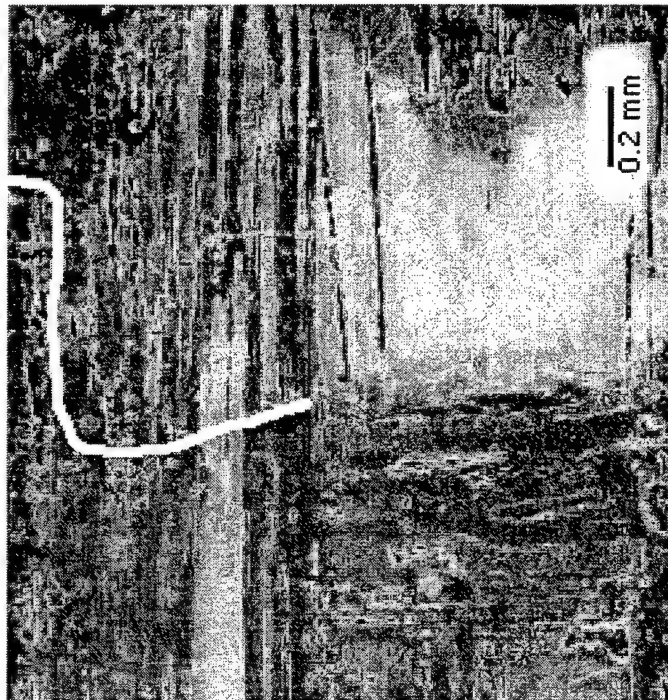


Fig. A2 8HSW/alumina specimen exposed to 1100°C for 146 hrs. in Argon. Analysis was made at $K = 19 \text{ MPa}\sqrt{\text{m}}$, or 95% of $K_c = 20 \text{ MPa}\sqrt{\text{m}}$. Left: Region analyzed. Crack is shown in white. Right: Mohr's circles of strain with edges of microstructural features shown as dotted lines.

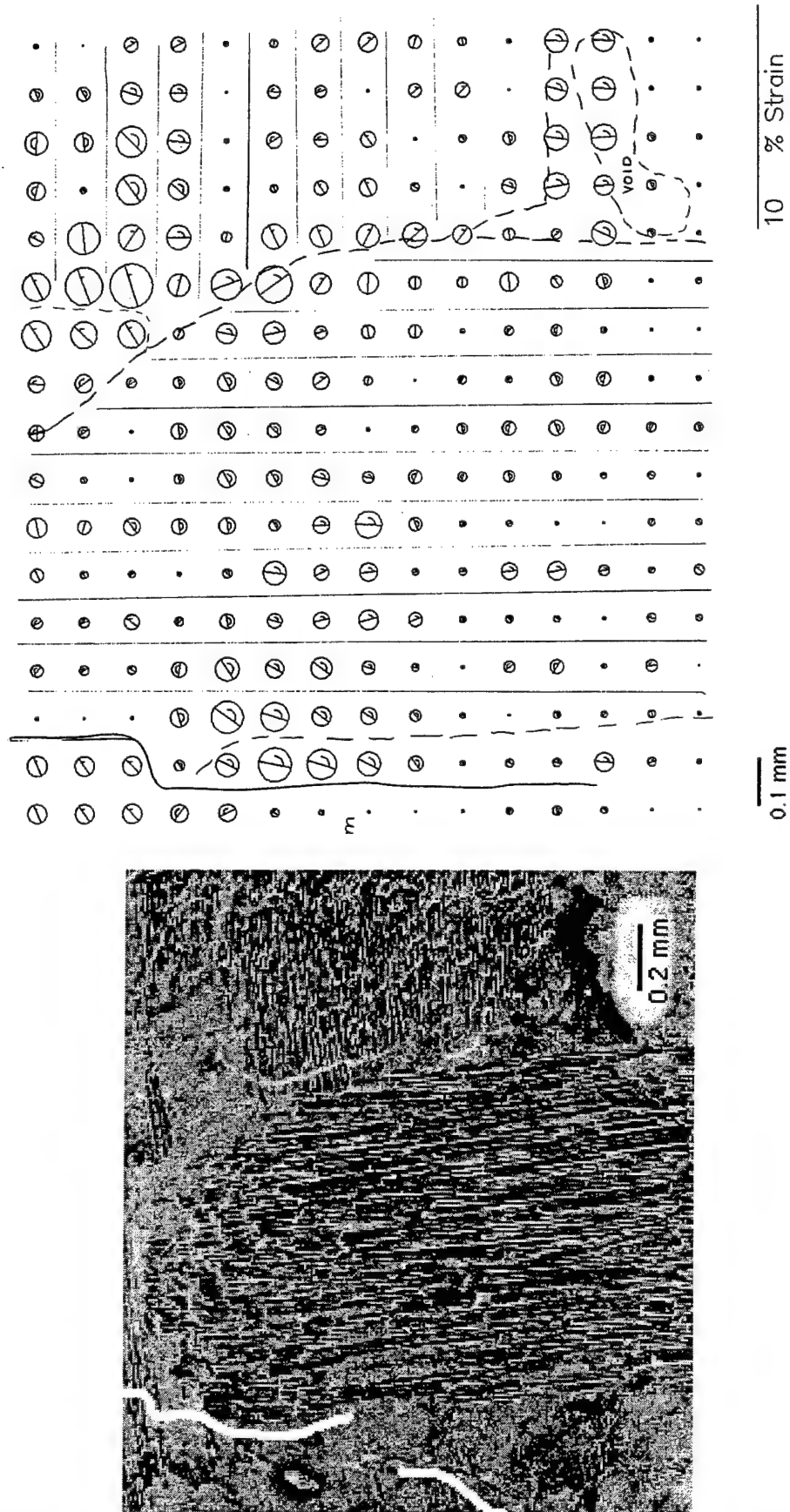


Fig. A3 8HSW/alumina specimen exposed to 1100°C for 146 hrs. in Argon. Analysis was made at $K = 14.2 \text{ MPa}\sqrt{\text{m}}$, or 77% of $K_{IC} = 17.7 \text{ MPa}\sqrt{\text{m}}$. Notch is about 1 mm above the top of the image. Left: Region analyzed. Crack is shown in white. Right: Mohr's circles of strain with edges of microstructural features shown as dotted lines.

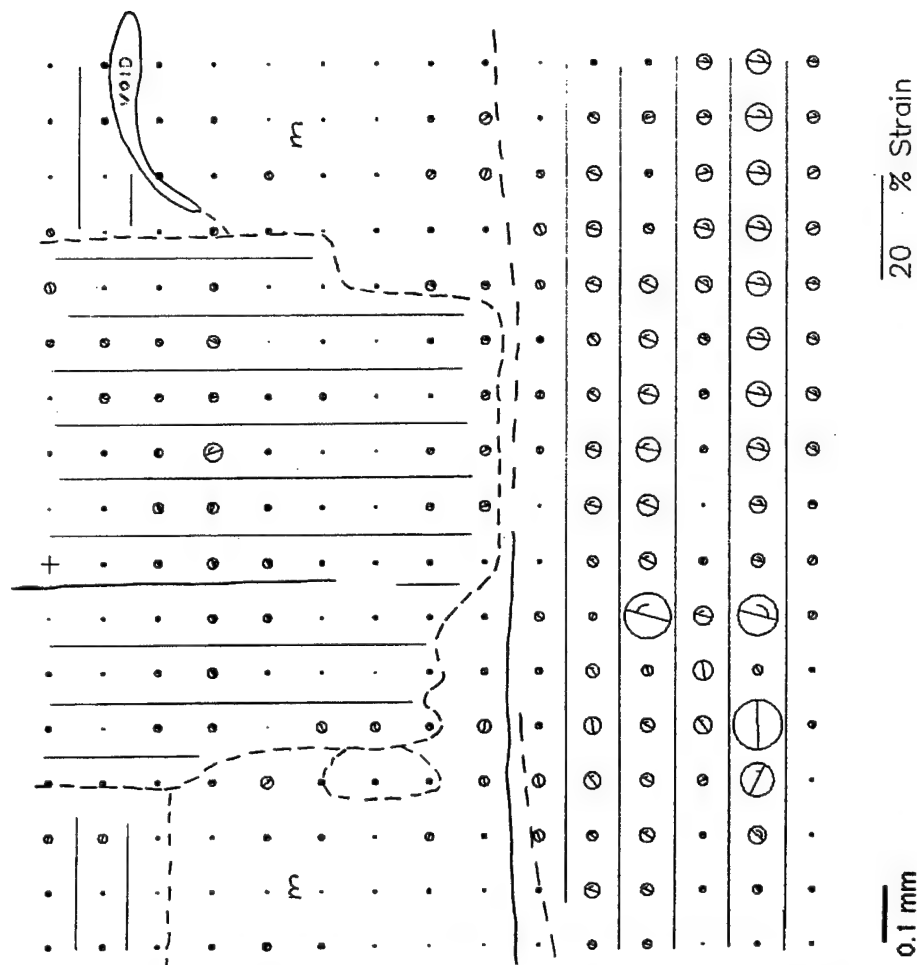
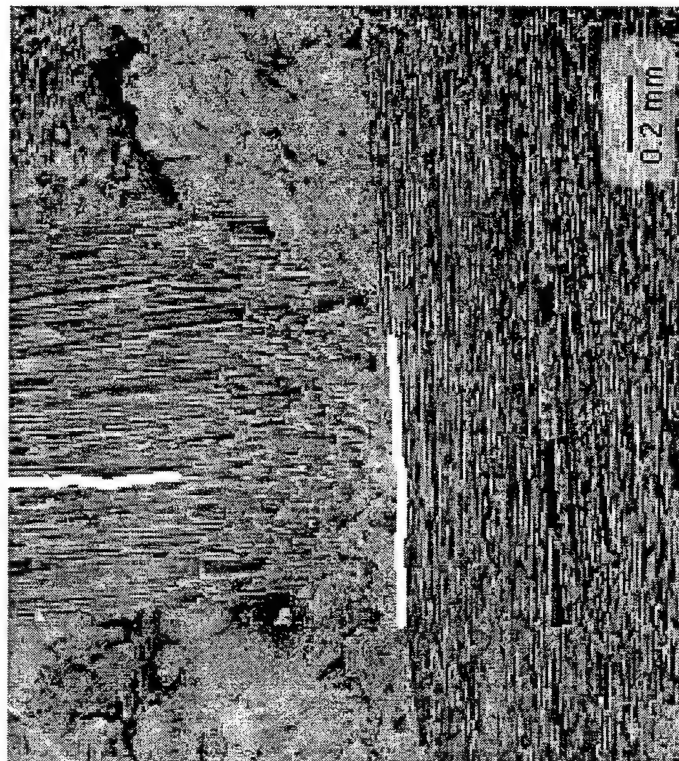


Fig. A4 8HSW/alumina specimen exposed to 1100°C for 146 hrs. in Argon. Analysis was made at 16.0 MPa \sqrt{m} , or 90% of K_{IC} = 17.7 MPa \sqrt{m} . Notch is about 1.5 mm above the top of the image. Left: region analyzed. Cracks are shown in white. Right: Mohr's circles of strain with edges of microstructural features shown as dotted lines. Fiber directions are shown.

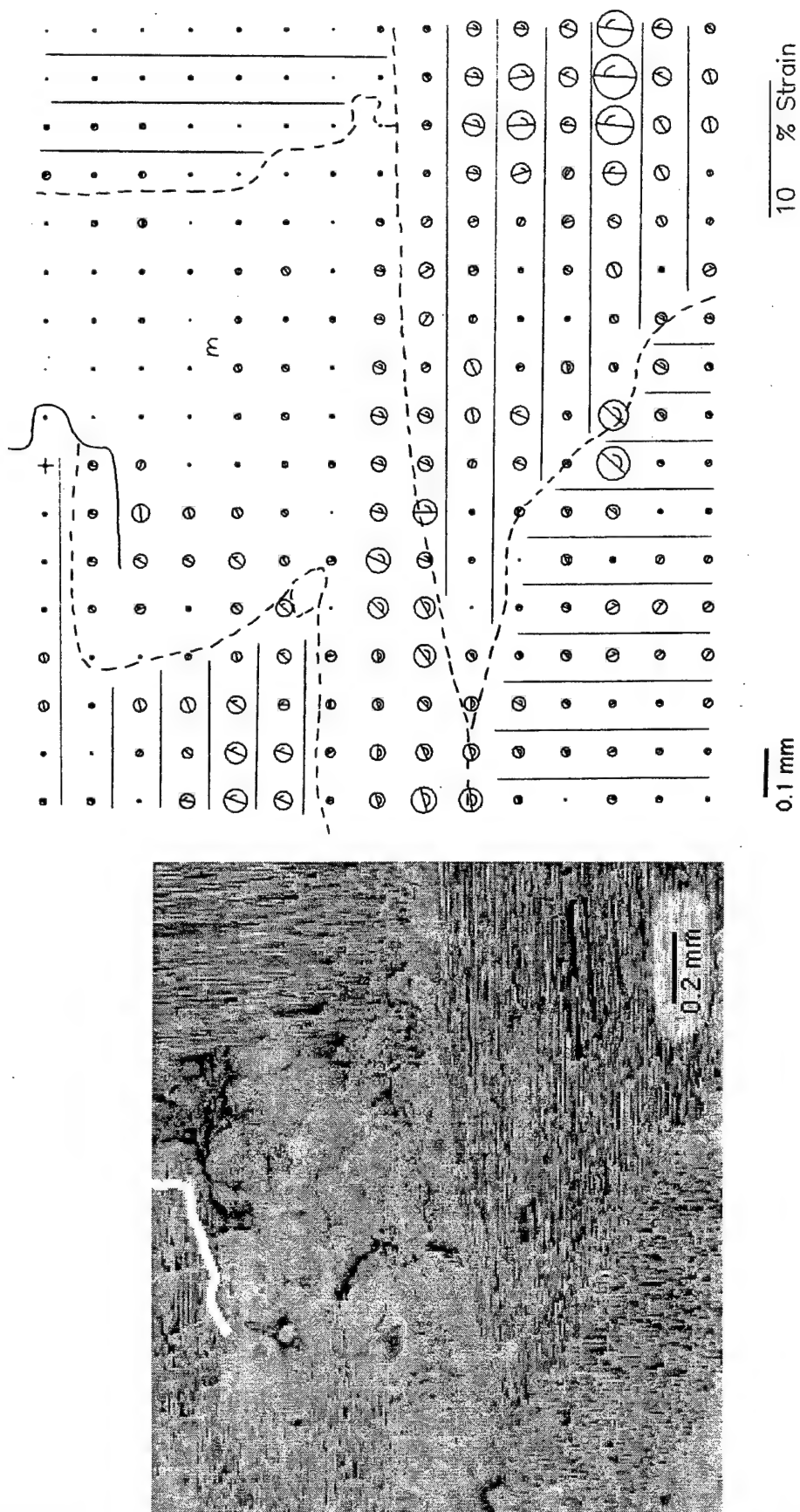


Fig. A5 8HSW/alumina specimen exposed to 1100°C for 146 hrs. in Argon. Analysis was made at $K = 16.8 \text{ MPa}\sqrt{\text{m}}$, or 95% of $K_c = 17.7 \text{ MPa}\sqrt{\text{m}}$. Notch is about 1.8 mm above the top of the image. Left: Region analyzed. Crack is shown in white. Right: Mohr's circles of strain with edges of microstructural features shown as dotted lines. Fiber directions are shown.

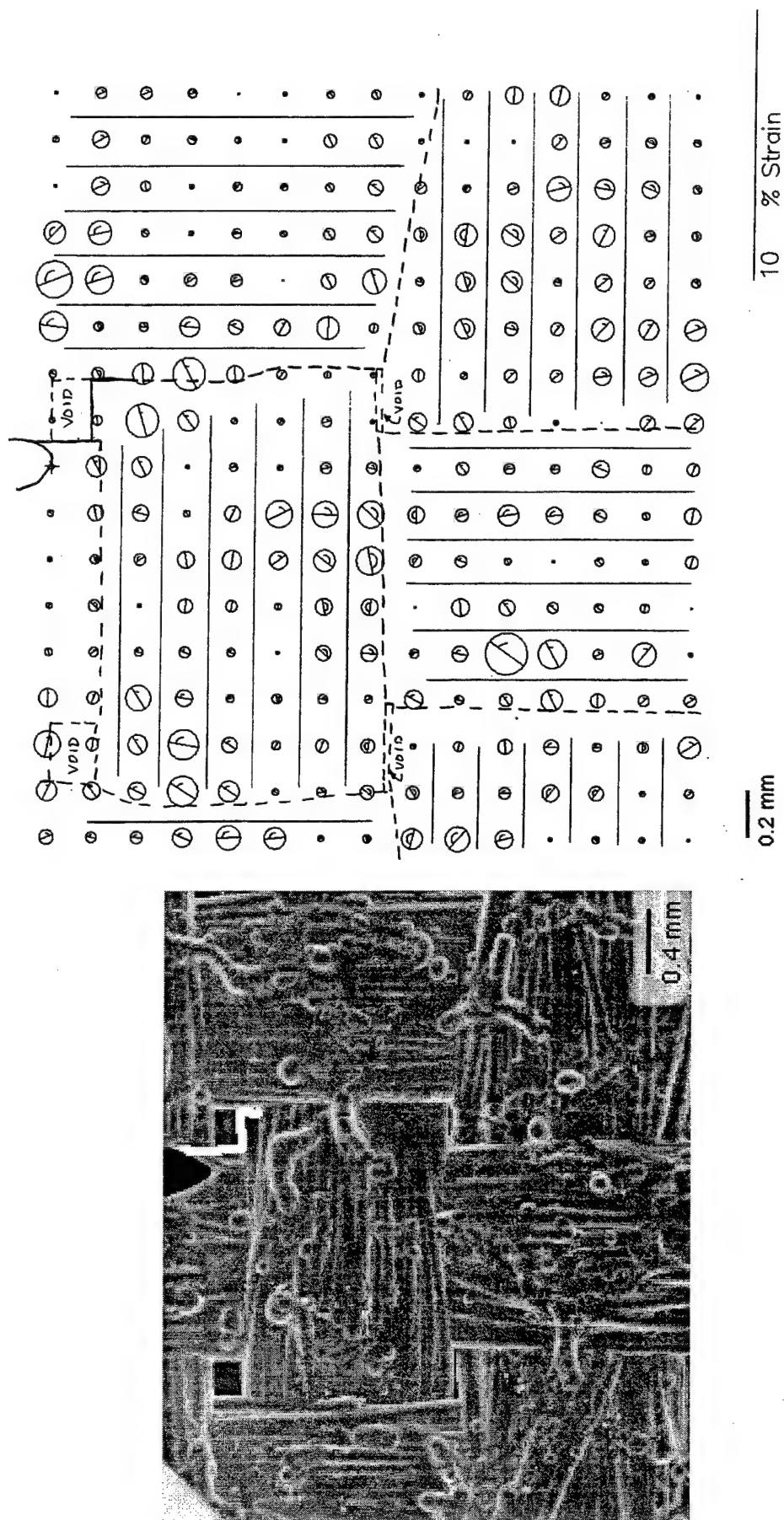


Fig. A6 PW/SiC specimen As Received. Analysis was made at $K = 12.0$ MPa \sqrt{m} , or 90% of $K_c = 13.4$ MPa \sqrt{m} . Left: Region analyzed. Crack is shown in white. Right: Mohr's circles of strain with edges of micro-structural features shown as dotted lines. Fiber directions are shown.

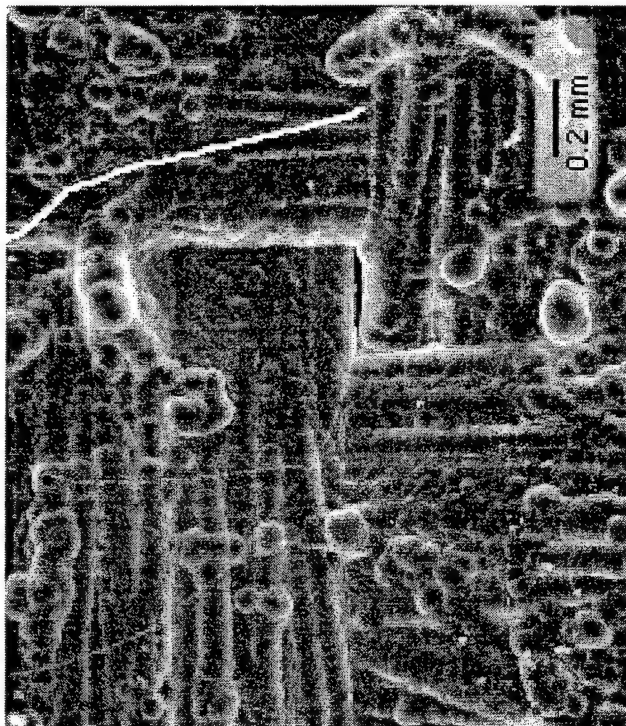
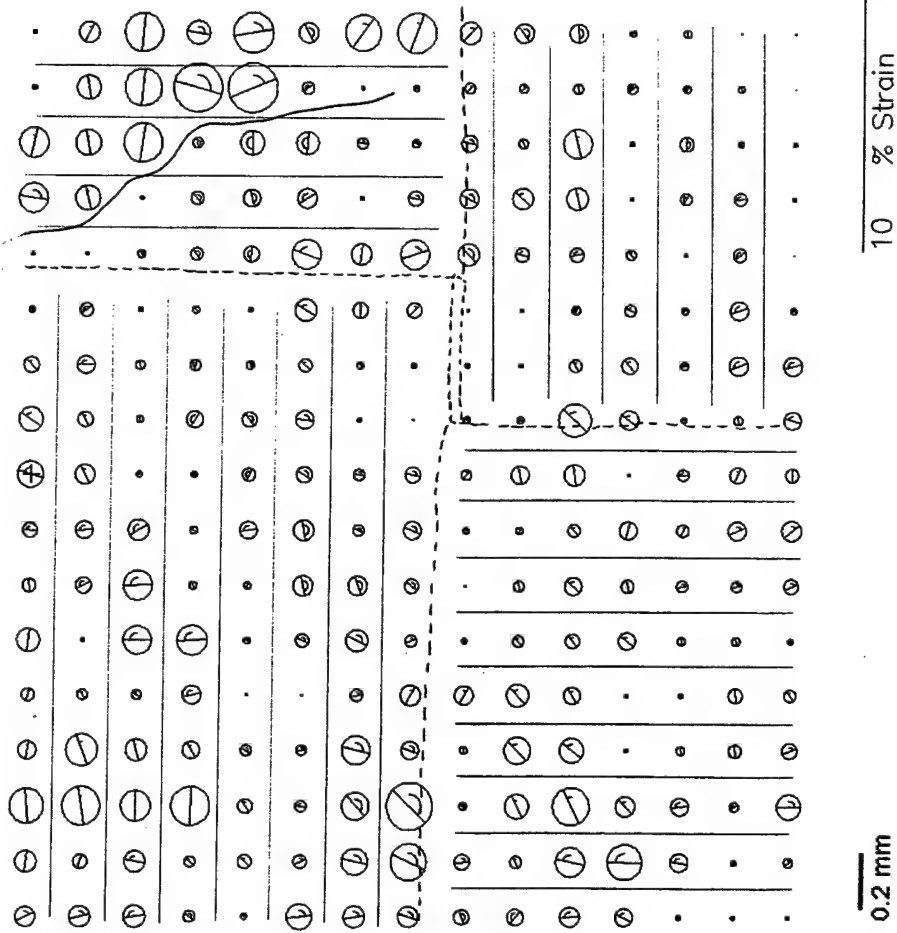


Fig. A7 PW/SiC specimen As Received. Analysis was made at $K = 13.0$ MPa \sqrt{m} , or 97% of $K_{IC} = 13.4$ MPa \sqrt{m} . Left: Region analyzed. Crack is shown in white. Right: Mohr's circles of strain with edges of micro-structural features shown as dotted lines. Fiber directions are shown.

FINITE ELEMENT MODELING OF FRACTURE TOUGHNESS IN FABRIC REINFORCED CERAMIC MATRIX COMPOSITES

Daniel P. Nicolella and David L. Davidson
Southwest Research Institute
San Antonio, TX 78228

ABSTRACT

A finite element model of a plain weave fabric was constructed to simulate the stresses and strains in a fabric containing a slit as it was loaded. The model simulated an experiment devised to measure the fracture toughness of fabrics. The model was also reconfigured to simulate the fracture of compact tension (CT) specimens similar to those used in an experimental micromechanics investigation. The dimensions of the fibers in the model were modified, and a matrix element was included, to simulate a plain weave fabric reinforced ceramic matrix composite (CMC) being loaded in a fracture toughness experiment. The results are consistent with many of the observations made during the fracture toughness evaluation of the CMC. The factors identified from this modeling process that control fracture toughness are the modulus and crushing strength of the matrix and the size of the fabric unit cell.

INTRODUCTION

Finite element methods (FEMs) have been used for many years to model woven fabric reinforced composites. Tan, Tong and Steven [1] have reviewed recently much of the work that has been done. A large proportion of the many analyses has been for the purpose of understanding and predicting the elastic properties, principally the elastic moduli and Poisson's ratio, of composites with woven, braided, and knitted fabric reinforcements. Some work has been done to predict thermal properties of these materials. Much less work has been done to predict the stress-strain and fracture properties. Naik and Ganesh [2] investigated the tensile failure of plain weave fabrics, but other failure processes, such as fracture toughness and fatigue failure, have not been modeled using FEMs. The purpose of this paper is to present results of a FEM model designed to investigate the fracture toughness of plain weave reinforced ceramic matrix composites. This model complements a similar model constructed

previously to investigate the fracture toughness of plain weave fabrics without matrices [3]. The modeling process was conducted parallel to an experimental micromechanics investigation of the fracture toughness of fabrics [3] and ceramic matrix composites (CMCs) [4].

MODEL

The model used to simulate fracture of ceramic matrix composites is unlike many of the models developed to predict the elastic response of CMCs. Those models have used a "unit cell" approach, while the present model uses a pinned-bar simulation of the fabric geometry.

In developing the computational model, an incremental approach was taken in which the initial model consisted of only the fabric [3]. However, the model was developed so that additional constituents (such as the matrix) could be added. Throughout the development of this model, its predictions were to be validated against experimental results to ensure its applicability.

The model takes advantage of the discrete nature of the fabric by modeling the fiber as linked beams and their intersections as joints. The model was first developed to simulate the fabric fracture toughness experiment [3]. To reduce computational cost, a one-quarter symmetry model was constructed taking advantage of the symmetry of the experiment and boundary conditions.

Fabric Model: The geometric configuration of the model was designed to simulate the experimental configuration. A one-quarter symmetry model was used taking advantage of the symmetry in the experimental configuration. The model consisted of an area of fabric with a slit on the vertical centerline splitting the model horizontally in the center. The finite element mesh consisted of slender beams representing the fibers of the fabric connected through rotational pin joints at each fiber intersection. The initial fabric model was for a plain weave and used fibers 0.5 mm in diameter and spaced 0.5 mm apart.

Fiber Elements: Individual fibers in the fabric were modeled as a slender beam with a circular cross section. Each beam was connected to its neighboring beam using pins joints that allowed in-plane rotation; the

bending stiffness of the beam is much greater than the rotational stiffness provided at each joint effectively creating a stiff beam. The general concept is shown in **Fig. 1**. The stiffness of the fibers in the fabric on which fracture toughness experiments were conducted was determined from load-elongation experiments performed on single fibers.

To model the fiber reinforced composite, the fibers were given dimensions approximating the fiber shape in the ceramic matrix composites that were experimentally evaluated. Fiber shapes were generally flat, having cross-sectional dimensions of approximately 1.5 mm by 0.2 mm. The spacing of the beams (flat fibers) was for this plain weave material approximately 3.0 mm. Thus, the "unit cell" of the material was 3 x 3 mm. Stiffness of the fibers (Nicalon) used in the composite material was determined from the literature [5].

Each beam representing a fiber in the model was connected by pinned joint; thus, individual fibers in the fabric were strings of short beams with a rotational joint at each fiber crossing. These elements provided displacement constraints between elements but allowed rotation relative to each other. Rotational stiffness at each pin joint was provided through non-linear rotational springs. The behavior of the springs is defined by the kinematic behavior of the joint. The torque-displacement behavior assumed for the fabric is shown in **Fig. 2**. An initial torsional stiffness provided for minimal rotational resistance between fibers, but when the rotation reached the lock-up angle (the angle where fibers begin to touch each other), the stiffness increases accordingly.

The fibers were allowed to slide across each other; i.e., to translate relative to each other at the fabric intersection points. While each fiber segment in both the horizontal (x), and the vertical (y) directions were connected via pinned joints, the vertical and horizontal fibers were connected to each other at their intersections via spring elements, thus allowing relative translation between the fibers. The stiffness of the spring, which simulated the sliding between fibers and is controlled by friction, was considered a parameter in the model. The appropriate behavior of the joint was determined by varying this friction parameter and comparing the model results to experimental results.

Composite Matrix: Matrix was included in the model by the addition of two dimensional, plane strain continuum elements. This matrix element was

connected to the fabric fibers as shown in **Fig. 3**. Each corner node was connected to either a vertical fiber node or a horizontal fiber node in an alternating manner so that the matrix provided shear stiffness to the model while allowing the fibers to slide relative to each other. An elastic-perfectly plastic material stress-strain behavior was used to describe the mechanical behavior of the matrix. When connected in this way, the matrix can also carry load, so this configuration is equivalent to assuming that the matrix is well bonded to the fibers.

The elastic modulus (E) and yield strength (H) were varied to determine the effect of matrix properties on fabric behavior. First, the bulk values of E and H were chosen for the matrix materials, SiC and alumina. But a mechanical microprobe had been used to measure values of E and H of these matrices in actual composites [5], so those values were used also in the model to better simulate the composites of interest. Table 1 lists the bulk values of E and H and measured "steady state" values, which occur at relatively large strains. The actual behavior is shown schematically in **Fig. 4**, and the assumptions used in the model are also shown.

Table 1
Matrix mechanical properties

Composite Fiber weave/matrix	Modulus (E) GPa	Hardness (H) GPa
<u>Bulk Ceramics</u>		
Alumina	386	15
Silicon carbide	390	24
<u>As-received Composite</u>		
8HSW/alumina matrix	150	5.8
PW/silicon carbide	51	3.3
<u>Composite after Exposure to 750°C for 64 hrs.</u>		
8HSW/alumina matrix	123	3.8
PW/silicon carbide	57	3.3

Boundary Conditions: Loads were applied to the boundary nodes of the fabric model on the edge opposite of the slit with magnitudes

corresponding to the hoop stress generated in the fabric by the blatter pressure. Nodes along the left edge of the model ($x=0$, the centerline of the test piece) were constrained via symmetry boundary conditions while the nodes along the bottom edge of the model were fully constrained. Nodes along the slit in the fabric were not constrained in their movement.

The model was solved using the commercial finite element analysis software package ABAQUS [6] to give stresses and strains at the nodes in each fiber element as load was increased. This has generated a large amount of data that has not yet been thoroughly analyzed, so the results given should be considered as preliminary.

RESULTS

The best way to include the elastic modulus and strength of the matrix in the model is not immediately clear, but after some consideration, the assumed material characteristics shown in Fig. 4 were used. Continuing with the incremental approach, the original fabric model (unit cell = 1×1 mm) was modified to include matrix elements, and E and H of the bulk ceramics were used. The effect of fiber sliding friction (k) were explored, but as can be seen in Fig. 5, the effect of changing matrix E is much larger than that of changes in fiber friction.

Shown in the Fig. 5, is the stress on the first fiber at the crack tip as a function of applied stress, defined as the load divided by the composite cross-sectional area. Fracture toughness is directly proportional to the applied stress, but the geometric factor for this configuration is not known, so fracture toughness was not used as the correlating parameter. Inserting a matrix in the fabric has caused a decrease in the stress on the first fiber because the matrix carries part of the applied stress, and the higher the magnitude of the modulus, the more stress the matrix carries.

Next, the model was modified to more closely match the ceramic matrix composites being evaluated by experimental micromechanics. Fibers in the CMCs were measured as being approximately flat, having a cross-section about 1.5×0.02 mm, with a unit cell of 3×3 mm. Results were obtained for the same loading as used in the fabric model, so they are comparable to Fig. 5. Fiber sliding friction $k = 0.13$, and $E = 400$ and 80 GPa were used in the model. The results are shown in Fig. 5. The figure shows, principally, the effects of changes in (H), which has been modeled

as the "yield" stress. The behavior of the model for $E = 400$ and yield (H) = 0.5 GPa is interesting. Evidently, stress on the first fiber is lowered, compared to a yield of 2 GPa, but so much deformation occurs in the fabric that the lock-up angle is exceeded, and the slope of the line increases as applied stress is increased further.

In reality, the matrix properties, as determined by pressing an indenter into the matrix away from fibers in the composite, initially are near those of the bulk ceramic (the value of the peak in Fig. 4), but as the indenter sinks farther into the matrix, it crushes the material, and both E and H drop to equilibrium values, listed in Table 1. This behavior can be modeled as having a high E , but a low yield stress, after which the material is perfectly plastic (has no work hardening or softening). This is a modification of the behavior shown in Fig. 4. Thus, for a specified value of applied stress, the effect of lowering the matrix crushing stress is to decrease the stress on the first fiber. This is equivalent to raising the fracture toughness of the material because the crack will propagate when the stress in the first fiber exceeds the level of stress that will fracture it. Since the applied stress must be raised to obtain a higher first fiber stress when the matrix crushing stress is lowered, this amounts to a higher fracture toughness resulting from a lower matrix crushing stress.

With this result, the model was modified from using the same boundary conditions as used for the fabric fracture toughness measurement to the configuration used in the micromechanics evaluation of the CMCs, which was a CT specimen. The model used a specimen with 60x60 mm overall dimensions and a value of 54 mm for the load-line to back-surface dimension.

The effects of applied stress on the first fiber stress are shown in Fig. 6 for the CT specimen model. In this case the correlating parameter is K , the stress intensity factor, because the geometric factor that relates K to load is known for CT specimens [7]. As with the first method of loading, the matrix assumes more of the stress when the modulus is the highest. Lowering the "yield" (crushing) stress of the matrix results in an even lower level of applied stress, which is equivalent to an increase in fracture toughness.

DISCUSSION

The assumptions used in the models show that inclusion of a matrix in the fabric raises the fracture toughness because the matrix carries load in addition to the fibers. Although this is a logical result, it has not yet been experimentally verified. However, the models, particularly that of the CT specimen, have captured many of the features identified with an experimental micromechanics evaluation of the fracture of plain weave fabric reinforced CMCs [4]. For example, experiments identified fibers moving relative to one another as an important aspect of the fracture process.

The reason for the enhancement of fracture toughness by a weak matrix is not completely clear, but it supports the hypothesis that matrix crushing allows the fibers to move relative to one another and better distribute the load, thereby lowering the load on the fiber at the crack tip, which raises the fracture toughness. Fiber motion creates something similar to a "plastic zone" in metals, which is the mechanism by which plasticity enhances fracture toughness in metals.

These models also allowed an examination of the effect of unit cell size on fracture toughness. The larger unit cell made up of larger fiber bundles was shown to support a higher applied stress for a given applied stress, which is indicative of a higher fracture toughness. This trend has not been verified experimentally, but it is a logical result. It would be interesting to change the model to incorporate fabric reinforcement with a satin harness weave, which has been shown experimentally to a higher fracture toughness than plain weave.

Another feature identified by the experimental micromechanics experiments as important in the fracture process was the deformation associated with voids in the composite. A method for including this feature in the model has not been found yet.

The magnitude of bonding between matrix and fibers has not been explicitly included in the modeling process. Perhaps the characteristics of modulus (E) and crushing strength (H) of the matrix that were used in the model have accounted for a weak interface between fibers and matrix, but that is not entirely clear. Further consideration of fiber-matrix

bonding and exploration of the modeling process is needed to examine this important issue.

CONCLUSIONS

1. The finite element model constructed to simulate the fracture toughness test for fabrics has successfully been applied to the simulation of ceramic matrix composites by altering the size of the fabric unit cell and including a matrix element.
2. The resulting model predicts trends in magnitude of stress on the fiber at the crack tip that correlate with observations made during an experimental micromechanics evaluation of the fracture process. The model also provides predictions for other features that could be examined experimentally.
3. The model correctly predicted that a porous matrix, i.e., one having a low crushing strength, would enhance fracture toughness, in comparison to a matrix with high crushing strength.

ACKNOWLEDGEMENTS

This research was funded by The Office of Naval Research, Dr. Steven Fishman project monitor, Contract N00014-96-C-0076.

REFERENCES

1. P. Tan, L. Tong and G.P. Steven, "Modelling for predicting the mechanical properties of textile composites - A review," Composites Part A, 1997, v. 28A, pp. 903-922.
2. N.K. Naik and V.K. Ganesh, "Failure behavior of plain weave fabric laminates under on-axis unitensile loading : I-Laminate geometry, II-Analytical predictions, and III-Effect of fabric geometry," J. Composite Mater., 1996, v. 30, pp. 1789-1856.
3. D.L. Davidson, D.P. Nicolella and B.S. Spigel, "The fracture toughness of fabrics as composite reinforcements" To be submitted to Experimental Mechanics

4. D.L. Davidson, "Fracture toughness micromechanics of fabric reinforced ceramic matrix composites" To be submitted to Journal of Materials Science.
5. G. Pharr and D.L. Davidson, "Matrix properties of fabric reinforced ceramic matrix composites as measured by mechanical microprobe," To be submitted to Journal of Composite Materials
6. ABAQUS v.5.6, HKS Inc., Pawtucket, RI.
7. ASTM Standard E399, Am. Soc. Testing and Mater.

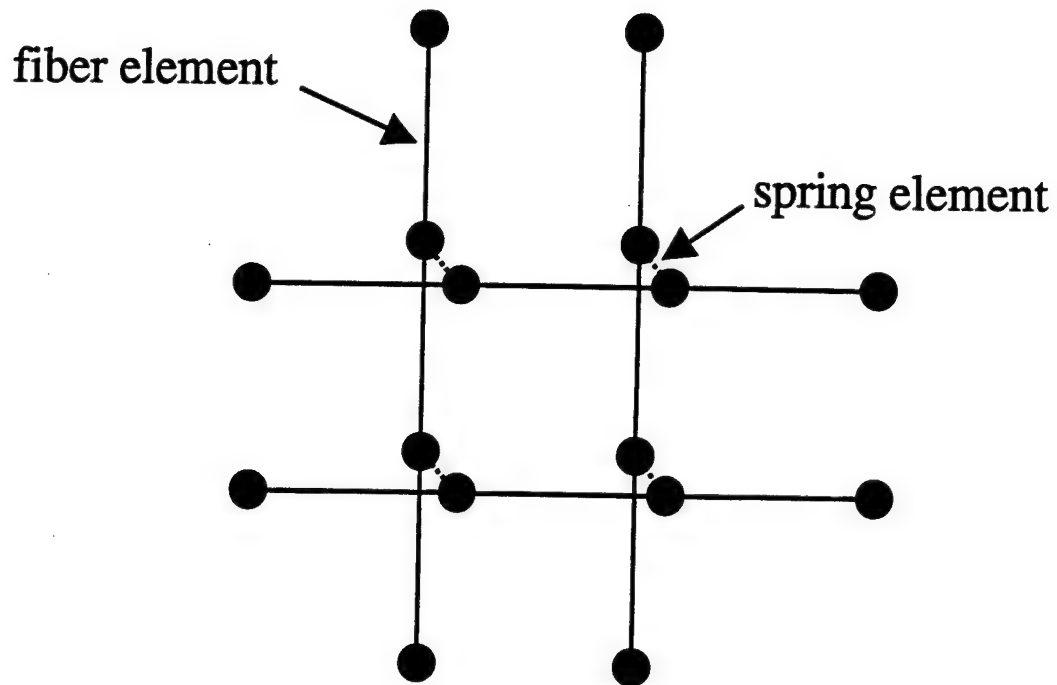


Fig. 1 Fabric model connectivity. A unit cell of plain weave fabric is shown. Where fibers cross each other, a pin joint was provided to connect the segments of fibers. At each fiber intersection, a spring element connected crossing fiber to simulate friction between the fibers. The nodes at the intersection of the fiber elements were coincidental in the actual model, but are shown offset in this illustration only for better visualization.

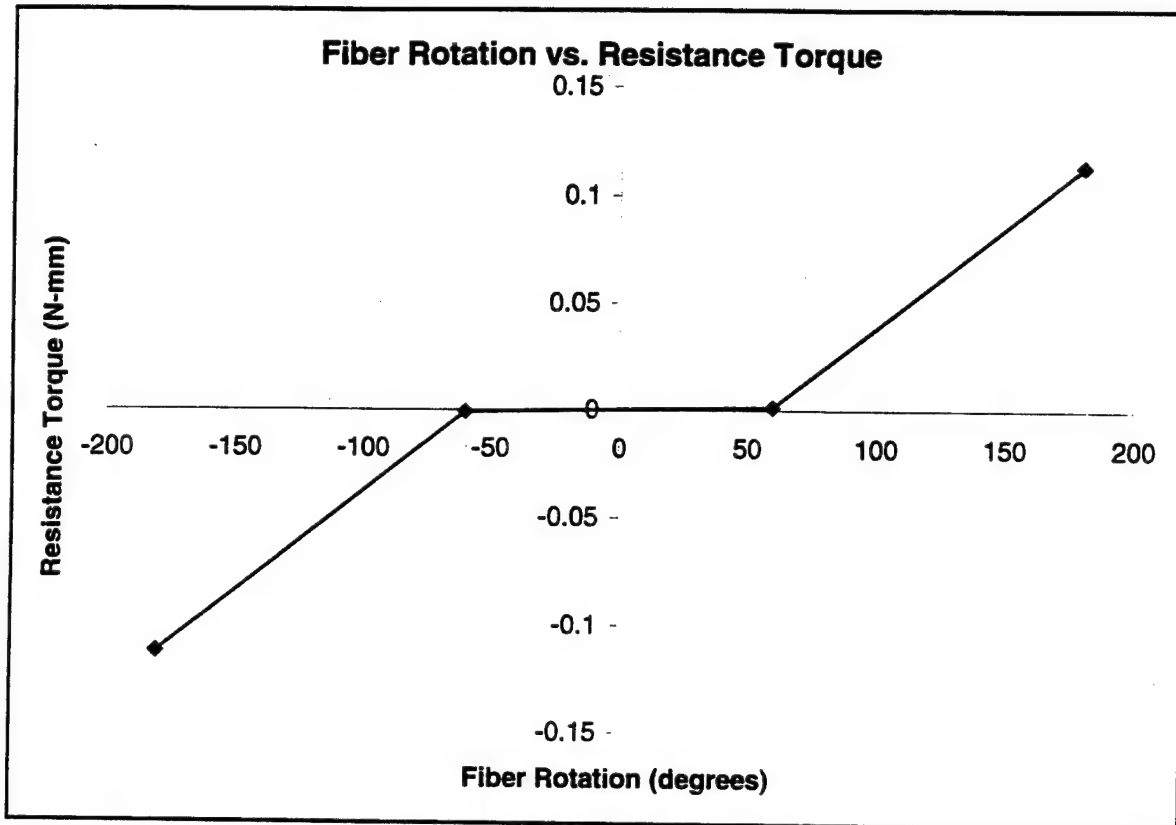


Fig. 2 Fiber Rotation vs. Resistance Torque. The fibers were allowed to rotate with respect to each other up to the lock-up angle (60° for the fabric model, 30° for the ceramic matrix composite) where the rotational resistance increased by a large factor.

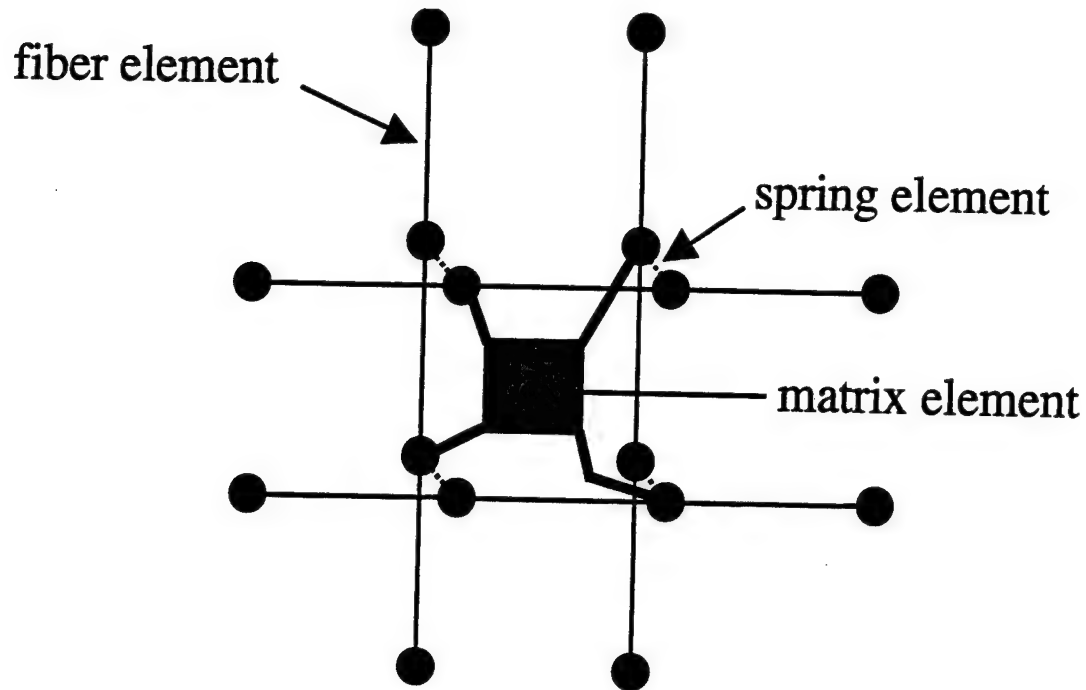


Fig. 3 Model of the composite showing how the matrix element was connected to the fiber elements. The connections are depicted by the dark lines. Note that the nodes at the intersecting fiber elements were coincident in the actual model, and are shown offset in this illustration only for better visualization.

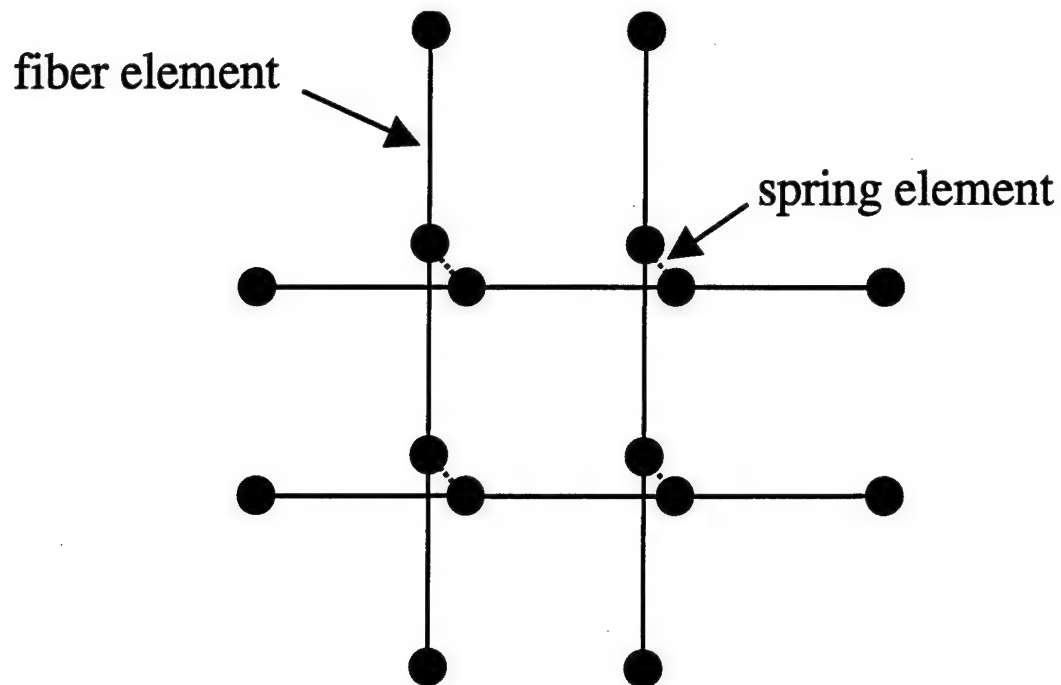


Figure 1. Fabric model connectivity. Note: the nodes at the intersection of the fibers are coincident in the actual model. They are shown offset for visualization purposes.

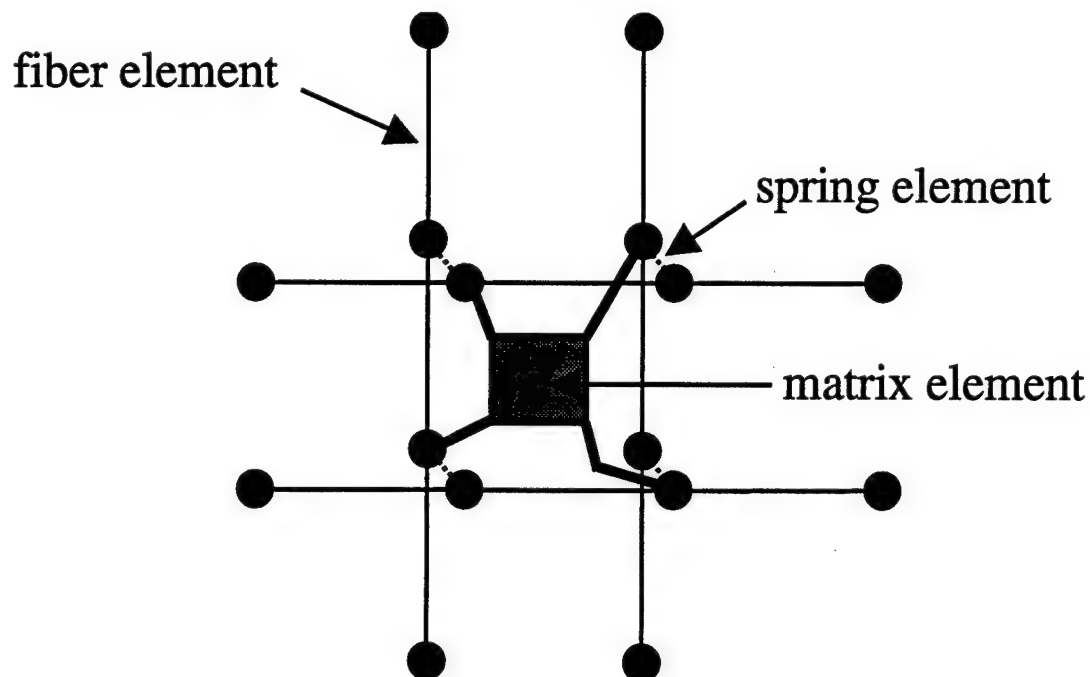


Figure 2. Composite model indicating the matrix connectivity. The matrix element nodes are related to the fiber nodes as indicated by the dark lines. Note: the nodes at the intersection of the fiber are coincident in the actual model. They are shown offset for visualization purposes.

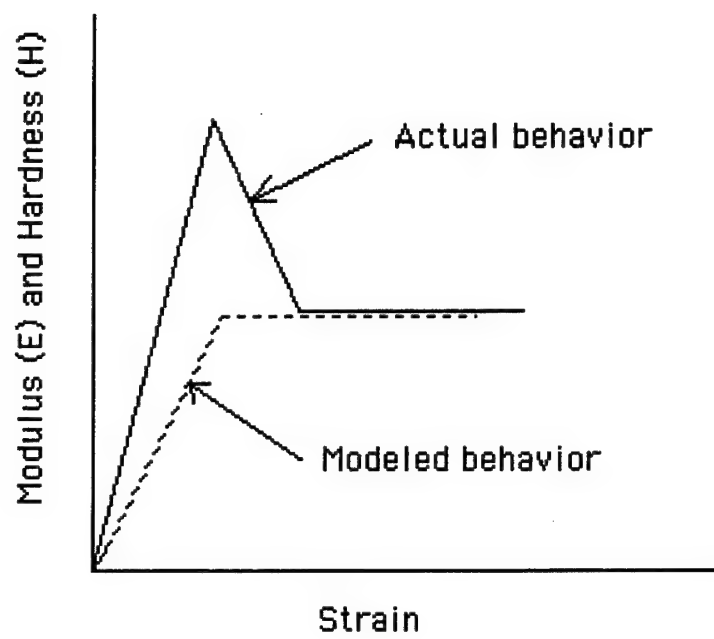


Fig. 4 Change in E and H with strain, as determined by mechanical microprobe.

Fabric Model

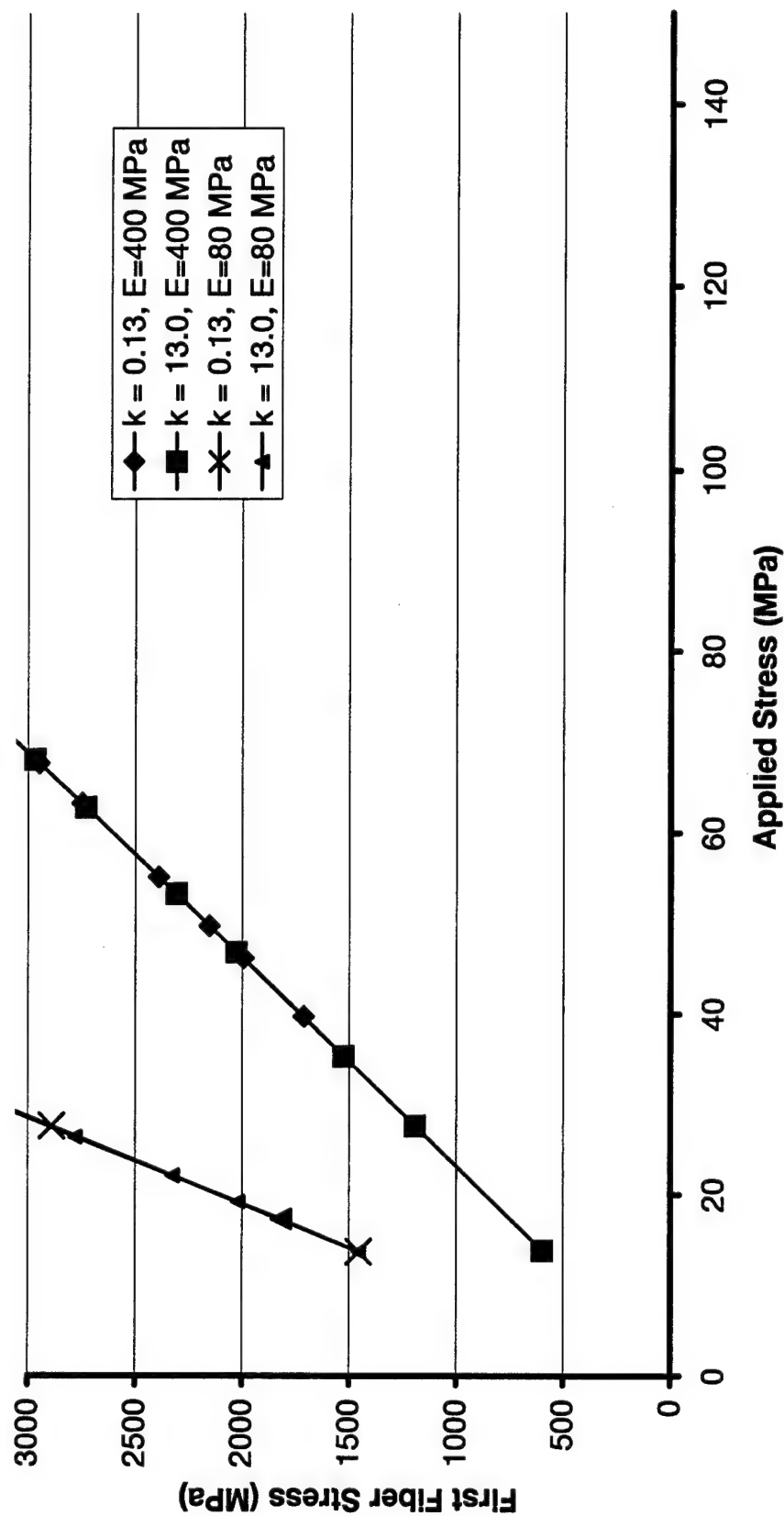


Fig. 5 Stress on the fiber at the crack tip as a function of applied stress using the fabric model with a 1x1 mm unit cell. The effect of inserting matrix in the fabric is shown for two values of E (matrix modulus). The effect of fiber friction (k) magnitude are also shown. Matrix yield stress used was 3.9 GPa.

Composite Fabric Model

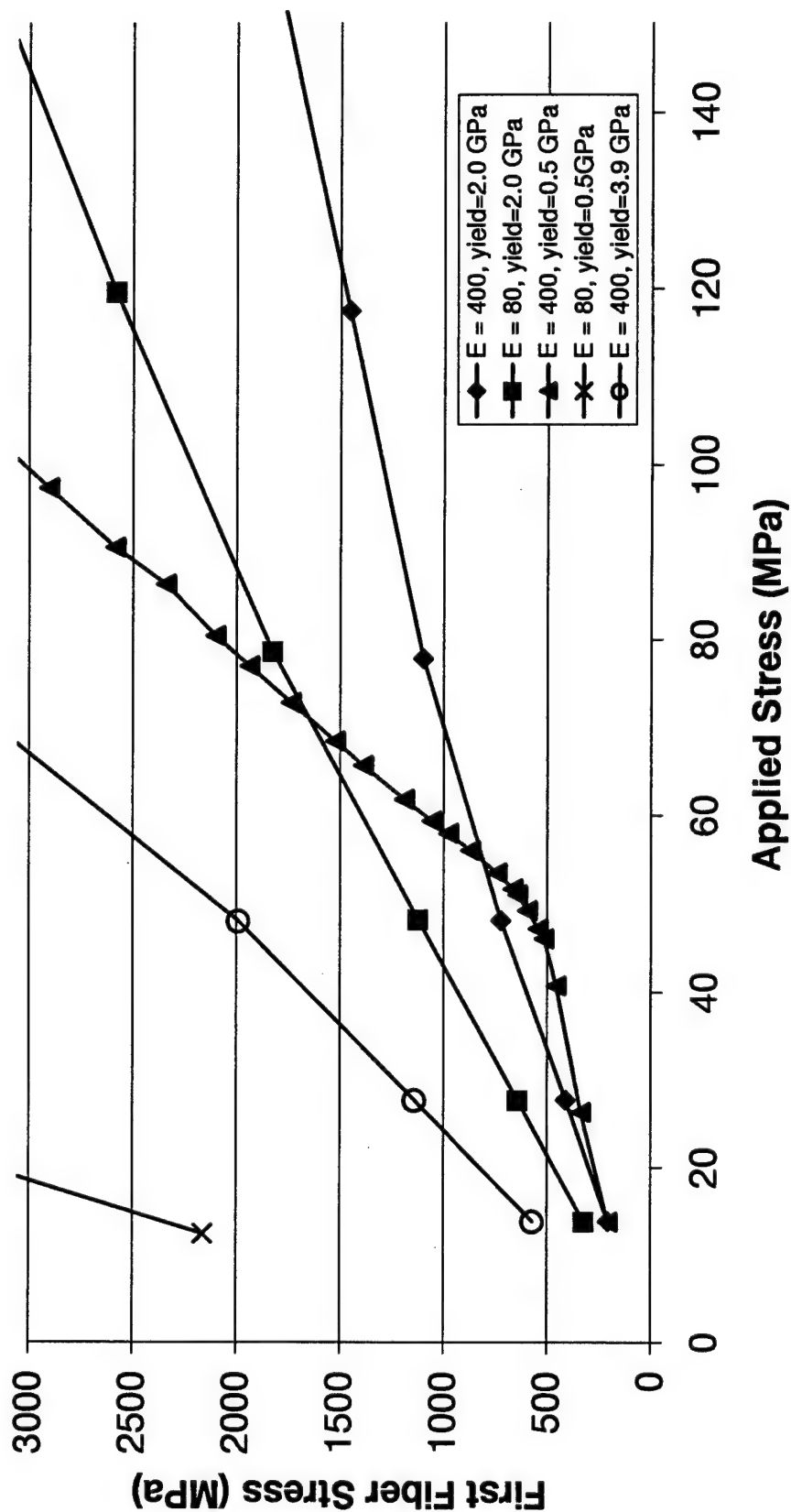


Fig. 6 Stress on the fiber at the crack tip as a function of applied stress using the fabric model with a 3x3 mm unit cell. The effects of changing E (matrix modulus) and matrix yield stress (H) are shown.

Fiber Reinforced Composite - CT Specimen Geometry

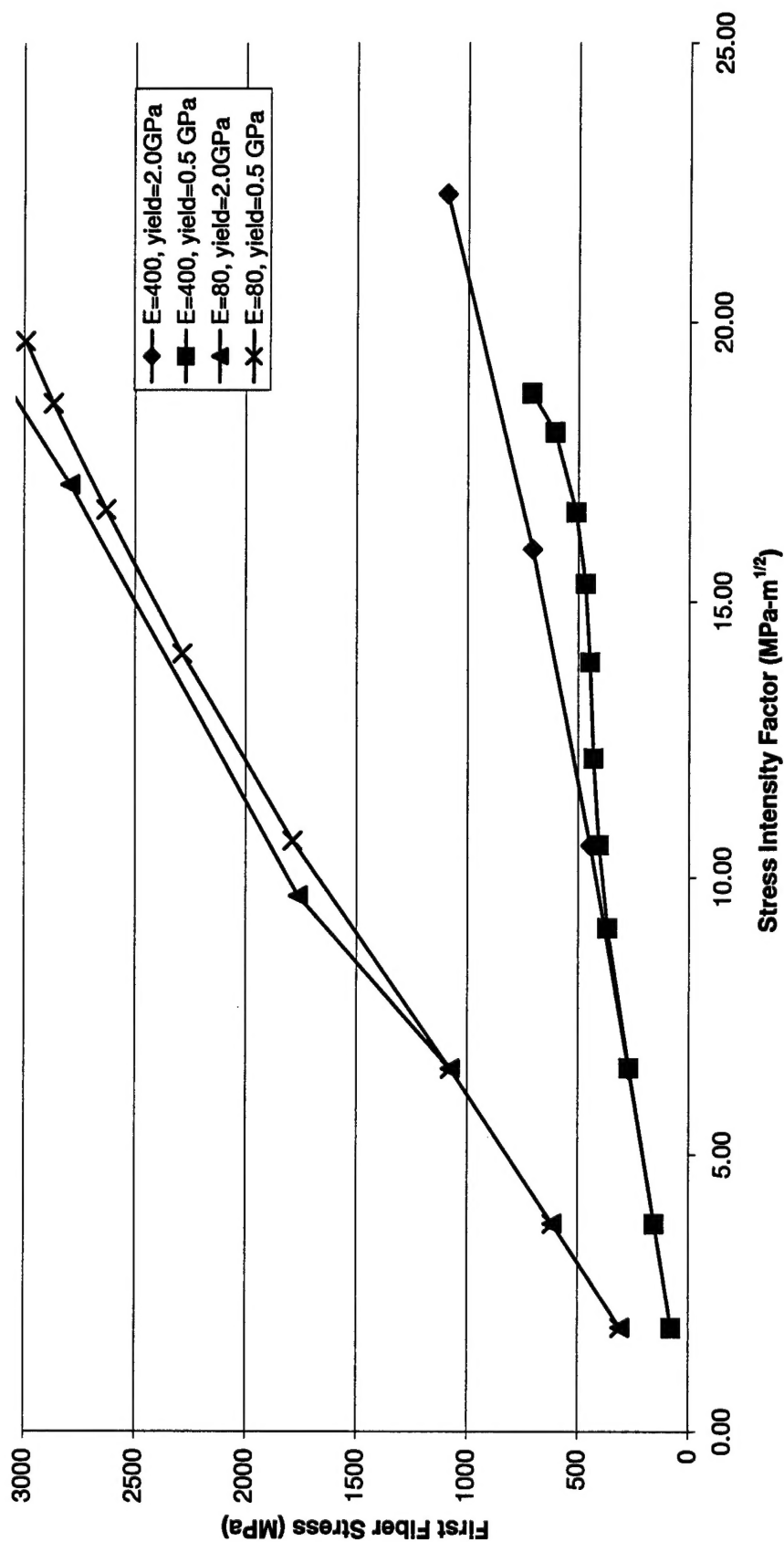


Fig. 7 Stress on the fiber at the crack tip as a function of stress intensity factor using a CT specimen model. The effect of matrix modulus and yield stress are shown.

CONCLUSIONS

The objective of this research has been to understand the fracture toughness of ceramic matrix composites so that they might be rationally designed from the constituent factors of the composite. From the results obtained, the following may be concluded:

1. Fracture toughness values $\geq 10 \text{ MPa}\sqrt{\text{m}}$ require the composite constituents to have the following material characteristics:

- Strong fibers
- Compliant matrix
- Weak fiber-matrix interface
- Reduced density; i.e., voids in the matrix.

2. Micromechanics experiments identified (a) fiber bundle relative motion as making a significant contribution to the fracture toughness of both the fabric (reinforcement) and the composites. The relative motion of fiber bundles in the composites is enhanced by a compliant matrix and voids in the material. Deformation around voids in the composite, was also shown to be an important feature of the fracture process.

3. A method for measuring the fracture toughness of reinforcing fabric was developed and validated for a low strength, plain weave fabric. If high strength fabrics can be similarly evaluated, then this method could provide a quality control assessment for fabric reinforcements used in ceramic matrix composites. It might also provide a quantitative assessment of the effects of fiber architecture (e.g., plain weave, 5HSW, twill, 8HSW, etc.) on fracture toughness, and possibly fatigue characteristics, of these composites.

4. A finite element model was constructed to simulate the fracture of fabrics, and a number of factors in the model were altered until the results of the model agreed with results obtained from an experimental micromechanics evaluation of fracture in fabrics.

5. Success with the fabric model led to construction of a finite element model for fracture of a CT specimen that incorporated many of the

features identified as important in the fracture process by the micromechanics investigation. This model requires further work, but can be used as a prototype in an effort to quantitatively identify the fabric and matrix characteristics that will enhance the fracture toughness of CMCs.

6. The characteristics of the composite constituents could be optimized to allow greater fracture toughness values to be obtained for CMCs. To optimize toughness, a somewhat more detailed model is required that will quantify the contribution of each factor to fracture toughness magnitude.

PUBLICATIONS

1. "THE FRACTURE TOUGHNESS OF FABRICS AS COMPOSITE REINFORCEMENTS" by D.L. Davidson, D.P. Nicolella, and B.S. Spigel: To be submitted to Experimental Mechanics.
2. FRACTURE TOUGHNESS MICROMECHANICS OF FABRIC REINFORCED CERAMIC MATRIX COMPOSITES" by David L. Davidson: To be submitted to Journal of Materials Science.
3. "MATRIX PROPERTIES OF TEXTILE REINFORCED CERAMIC MATRIX COMPOSITES AS MEASURED BY MECHANICAL MICROPROBE" by G. Pharr and D.L. Davidson: To be submitted to Journal of Composite Materials.
4. "FINITE ELEMENT MODELING OF FRACTURE TOUGHNESS IN FABRIC REINFORCED CERAMIC MATRIX COMPOSITES" by Daniel P. Nicolella and David L. Davidson: In preparation.